Universitat de Girona

Facultat de Ciències

Memòria del Treball de Fi de Grau

Títol del treball:

Implementation of a fast method for the evaluation of the effect of external electric fields on catalysis

---

Nom estudiant: Guillem Pey Costa

Correu electrònic: gpeycosta@gmail.com

Grau en Química

Nom del tutor: Dr. Josep Maria Luis Luis

Correu electrònic: josepm.luis@udg.edu

LUIS LUIS JOSEP MARIA - 43674128A

Firmado digitalmente por LUIS LUIS JOSEP MARIA - 43674128A

Fecha: 2023.07.04 09:15:16 +02'00'

Data de dipòsit de la memòria: Dimarts, 4 de juliol de 2023

Contents

Resum

La concentració de CO_2 durant l'últim segle ha augmentat exponencialment. El problema rau en l'alta eficiència del CO_2 d'absorbir i re-emetre la radiació IR a la superfície terrestre. Tot i que el CO_2 és el més problemàtic, n'hi ha d'altres que també tenen aquesta capacitat i es coneixen com els gasos d'Efecte Hivernacle. Com a conseqüència de l'alta concentració d'aquests en l'atmosfera, la radiació no pot escapar i es queda atrapada provocant que la temperatura global mitjana augmenti.

De la mateixa manera que les plantes utilitzen la fotosíntesi per a reduir el CO_2 en glucosa, la química moderna ha desenvolupat un procés, anomenat fotosíntesi artificial, que utilitza un catalitzador per a transformar el CO_2 en un altre producte de major interès, com per exemple el metanol. En aquest treball, s'estudia un mecanisme de dismutació del CO_2 en monòxid de carboni, el producte d'interès, i carbonat catalitzat per un complex de cobalt. Degut a l'alta estabilitat del CO amb el centre metàl·lic es genera un pou de potencial que impedeix que la catàlisi es pugui donar repetidament i s'aturi al primer cicle.

Altrament, l'aplicació de camps elèctrics en sistemes químics pot induir la catàlisi d'una reacció, o inhibir-la, i fins i tot afectar la selectivitat de la mateixa. Amb el mètode FDB_β es pot modelitzar computacionalment l'efecte dels camps elèctrics només calculant les propietats elèctriques (moment dipolar, polaritzabilitat, ...) de les molècules implicades. Matemàticament es basa en expandir en sèrie de Taylor de l'energia electrònica dependent del camp, on els coeficients son les propietats elèctriques. Llavors, per a definir la termoquímica d'una reacció es resten les respectives expansions dels productes (estats de transició) i reactius seguint l'estequiometria de la mateixa.

En aquest treball s'ha demostrat que el mètode FDB_β resulta ser una eina excel·lent per a l'estudi de l'efecte dels camps elèctrics. En la mateixa línia, s'ha desenvolupat un programa escrit en FORTRAN95 capaç de trobar el camp electric òptim per a assolir un valor preestablert per a una barrera o energia de reacció.

Mitjançant el mètode FDB_β s'ha estudiat l'efecte d'un camp elèctric en la catàlisi la reducció catalítica del CO_2 a CO estudiada en aquest treball. S'ha trobat que l'efecte d'un camp positiu en l'eix Z afavoreix l'alliberament del CO. Per altra banda, l'aplicació d'un camp elèctric negatiu en l'eix Y, tot i inhibir el procés anterior, afavoreix la cinètica de la reacció estabilitzant l'estat de transició que determina el TOF.

Resumen

La concentración de CO_2 durante el siglo pasado ha aumentado exponencialmente. El problema yace en la alta eficiencia del CO_2 de absorber y remitir la radiación IR a la superficie terrestre. Aunque este sea el más problemático, hay de otros que comparten la misma característica y se conocen como gases de Efecto Invernadero. Como consecuencia de tener una alta concentración de éstos en la atmósfera, la radiación no puede escapar y se queda atrapada provocando que la temperatura global media aumente.

De la misma manera que las plantas utilizan la fotosíntesis para reducir el CO_2 a glucosa, la química moderna ha desarrollado un proceso, llamado fotosíntesis artificial, que utiliza un catalizador para transformar el CO_2 en otro producto de mayor interés, como por ejemplo el metanol. En este trabajo se estudia un mecanismo de desproporción del CO_2 en monóxido de carbono, el producto de interés, y carbonato catalizado por un complejo de cobalto. Debido a la alta estabilidad del CO con el centro metálico se genera un pozo de potencial que impide la catálisi se pueda dar repetidamente y se detenga en el primer ciclo.

Paralelamente, la aplicación de campos eléctricos en sistemas químicos puede inducir la catálisis de una reacción, o inhibirla, e incluso afectar a la selectividad de la misma. Con el método FDB_β se puede modelizar computacionalmente los efectos de los campos eléctricos solo calculando las propiedades eléctricas (momento dipolar, polarizabilidad, ...) de las moléculas implicadas. Matemáticamente se basa en la expansión en serie de Taylor de la energía electrónica dependiente del campo, donde los coeficientes son las propiedades eléctricas. Para definir la termoquímica de una reacción se restan las respectivas expansiones de los productos (estados de transición) i reactivos siguiendo la estequiometría de la misma.

En este trabajo se ha demostrado que el método FDB_β resulta ser una herramienta excelente para el estudio del efecto de los campos eléctricos. En la misma línea, se ha desarrollado un programa escrito en FORTRAN95 capaz de encontrar el campo eléctrico óptimo para un valor preestablecido de barrera o energía de reacción.

Mediante el método FDB_β se ha estudiado el efecto del campo eléctrico en la catálisis de la reducción catalítica del CO_2 a CO es investigada en este trabajo. Se ha encontrado que el efecto de un campo positivo en el eje Z favorece la liberación del CO. Por otro lado, la aplicación de un campo en Y, aunque dificulta el proceso anterior, favorece la cinética de la reacción estabilizando el estado de transición que determina el TOF.

Abstract

The concentration of CO_2 has over the past century increased exponentially. The core of the issue lies in the high efficiency of CO_2 to absorb and remit IR radiation back to Earth's surface. Although CO_2 is the main responsible, there are other gases sharing the same characteristic and they are known as Greenhouse Gases. As a consequence of having a higher concentration of them in the atmosphere, the IR radiation cannot escape and is kept inside leading to a higher mean global temperature.

In the same way plants use photosynthesis to reduce CO_2 to obtain glucose, modern chemistry has developed a process known as artificial photosynthesis, that uses a catalyst to transform CO_2 into other high-interest products, such as methanol. This work studies a disproportionation mechanism of CO_2 into carbon monoxide, our interest product, and carbonate catalysed by a cobalt complex. Due to CO's high stability with the metallic centre, a potential well is generated which hinders a second catalytic turn.

On the other hand, the appropriate application of electric fields into chemical systems can induce the catalysis of a reaction, or inhibit it, and even affect the selectivity. With the FDB_β method, the effect of electric fields can be computationally modelled by only computing the electric properties (dipole moment, polarisability, ...) of the involved chemical species. Mathematically, it is based on the Taylor series expansion of the field-dependent electronic energy, where the coefficients are the electric properties. Then, to define the reaction's thermochemistry the expansions of products, or transition states, and reactants are subtracted following its stoichiometry.

In this work, it has been demonstrated that the FDB_β is an excellent tool to study the effect of electric fields on reactivity. Furthermore, we have developed a FORTRAN95 code capable of finding the minimum electric field required to impose a preestablished barrier or energy reaction.

By means of the FDB_β the effect on catalysis of an electric field has been studied on the catalytic reduction CO_2-to-CO studied in this work. On one hand, it is found the effect of a positive electric field on the Z axis favours the CO release. In contrast, although the effect of a negative field on the Y axis hinders the previous process, it enhances the kinetics of the reaction stabilising the formation of the transition state that determines the TOF.

A brief note on sustainability

Computational Chemistry is one of the big four branches of Chemistry, together with analytic, inorganic, and organic. In this discipline computers are used to study and understand the structure of the molecules and reaction mechanisms, among other things. Therefore, we do not need to use halogenated solvents nor cope with residues, thus, one could say it is the cleanest and safest field of Chemistry.

In my Final Degree Project, I am studying the reduction of CO_2 to CO catalysed by External Electric Fields. Although CO is not a hydrocarbon, it is a relevant C_1 platform widely used in industrial processes such as the Fischer-Tropsch synthesis of hydrocarbons or carbonylation reactions. Using this transformation, there is the possibility of reducing the Greenhouse Effect generated by CO_2.

Thoughts on the ethics in the field of Computational Chemistry

Lately, Computational Chemistry has become a powerful tool for the development of technologies, of renewable energies even in medicine. Nevertheless, this branch of Chemistry is not exempt from ethical dilemmas.

One of the simplest cases of mala praxis is the manipulation of results or data falsification. Even though they can be proven, it could take several days or weeks to either confirm or retract them. As a consequence, it has appeared what is known as a "Replication Crisis" where scientific works are almost unrepeatable, contradicting one of the cornerstones of the scientific method. On these grounds, the scientific work's reputation could be questioned or even considered fraudulent. In this study we provide all the tools and methods to replicate all the results that are presented.

Comment on women's underrepresentation in science

Gender bias and women's underrepresentation in science is a problem that has been carried on for more than a century. Women are usually the minority in research groups and due to this fact, it is less likely they earn funding or achieve higher power, or ranking, positions.

Low women's representation in science leads to a scenario where younger women are lacking role models to pursue a career in science. With the aim of solving the matter, encouraging women into science is a goal of the future, which the current generations should have in mind for the sake of diversification. Fortunately, computational chemistry is a field where women are achieving important success, being the first step to reducing women's underrepresentation in science.

1 Introduction

It is undeniable the fact that, during the late 19^{th} Century and the whole 20^{th} Century, the concentration of CO_2 in the atmosphere has increased due to several reasons related to worldwide industrialisation such as the combustion of fossil fuels[1][2]. Considering that they are not renewable sources of energy, the accelerating demand for energy leads to an increasing consumption of these fuels thus directly pointing to an energetic crisis. Nowadays, this growth is still a problem simply because it keeps increasing every year.

A common important feature of this gas, and other of similar properties, such as water vapour, methane, nitrous oxide, and ozone[3], is that it absorbs IR radiation in a wide range of frequencies and then emits it back to Earth's surface[4]. When the concentration of these types of gases remains within natural thresholds, they are responsible to keep the planet at a stable temperature throughout the season. The IR radiation absorbed by greenhouse gases is trapped into the Earth's atmosphere and the average temperature of the planet increases over the natural limits[5]. The excess of IR radiation in the atmosphere related to the increase in temperature is known as the Greenhouse Effect.

Taking everything into consideration, mankind has been releasing for over 100 years astronomical quantities of methane and carbon dioxide to the atmosphere. This sudden increase of concentration in the atmosphere has caused these greenhouse gases to send back IR radiation to the surface rising, the Earth's temperature, several degrees Celsius within a short time span[1].

Based on quantum theory concepts, the energetic difference between the HOMO and LUMO orbitals is a good indicator of the reactivity of a molecule[6]. For carbon dioxide, the HOMO-LUMO gap is rather large ($\sim$ 228.36 kcal/mol) which gives it a huge stability, thus low reactivity. As a consequence, CO_2 is a difficult molecule to activate. It is also known that the Grignard reagents with CO_2 in acid media are used to generate carboxylic acids[7]. However, they involve harsh reaction conditions that are not pragmatic to implement on a large scale to reduce the CO_2 levels in the atmosphere.

From this point of view, there are two alternatives: relying on greener sources of energy not based on fossil fuels, or activating the emitted CO_2 and transforming it, ideally, into other higher-value products with the ultimate goal of removing it from the atmosphere. The first scenario implies finding other cleaner chemical reactions that do not use combustion, consequently avoiding the production of this gas at all. The second one relies on the efficient, and green, activation of this molecule to obtain simple alcohols or even fuels. To achieve this difficult goal, one must rely on catalysis.

The definition of catalysis is to increase the rate of a reaction *via* a substance, known as a catalyst, which is not consumed during the reaction and remains unchanged after it. At the molecular level, if the catalyst is homogeneous, as in this work, its recovery enables the catalyst to participate multiple times in the activation of the reactants in a cyclic scheme, known as the catalytic cycle.

Within the context of energy production, there is a basic statement to always take into account: chemical energy is stored in chemical bonds through an endothermic reaction. Therefore, the most straightforward way to gain access to it is through an exothermic reaction.

As an example, the simplest, and greenest, reaction is the endothermic decomposition of water into molecular hydrogen and oxygen followed by the exothermic, and spontaneous, recombination to

[1] `https://climatechangetracker.org/global-warming/yearly-average-temperature`

generate water (see Figure (1)).

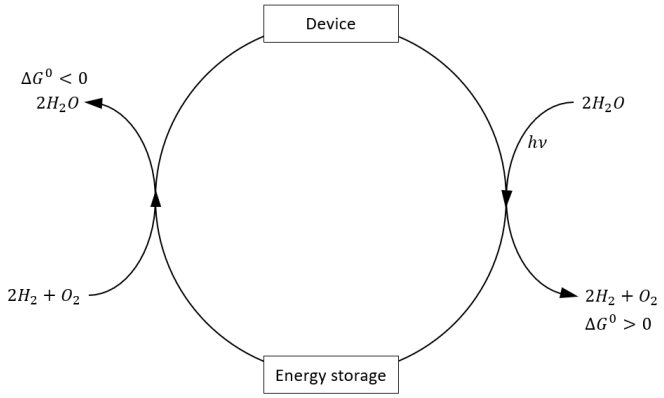

Figure 1: Production of green energy by the decomposition of water into molecular hydrogen and oxygen.

Nevertheless, the first reaction only takes place with the help of a photocatalyst, or an electrocatalyst if electrodes are used. Ideally, it is wanted to use a photocatalyst as the extra energy required for the dissociation is given by the sunlight, a green source of energy.

This reaction has already been studied extensively both experimentally and computationally. One of the first examples of photo-catalysis, using 1^{st}-row transition metal complexes, was developed by Chen[8] and coworkers with a cobalt complex using a pentadentate aminopyridine-based ligand ($Py_2{}^{Ts}$tacn). A few years later Lloret-Fillol and Call[9] tested variants of the same catalyst on the reduction of ketones in the presence of water to compare efficiencies; the very next year Lloret-Fillol used a tetradentate variant of the same catalyst ($^{X,Y}Py^{Me}$tacn) as Chen obtaining promising results[10] on the same context.

Another alternative to tackling the problem regarding the energetic crisis is what has been previously mentioned: transforming the released CO_2 by an unfathomable amount of processes to the atmosphere to generate other non-harming high-interest products such as HCO_2^- or CO_3^{2-} anions, or the specific case of this work carbon monoxide.

The CO molecule is not considered a greenhouse gas, as opposed to carbon dioxide, because it is not as efficient at absorbing IR radiation[3]. This comes with a double advantage: on one hand, reducing the Greenhouse Effect and, on the other hand, obtaining a relevant C_1 platform widely used in industrial processes such as the Fischer-Tropsch synthesis of hydrocarbons[11][12] or carbonylation reactions.

Nature already copes with the activation of CO_2 into other reduced carbon species such as glucose employing solar light (photosynthesis), thus a green transformation. The equivalent procedure without using natural substances but organometallic complexes is referred to as Artificial Photosynthesis (AP).

In this regard, AP has already been studied but either the catalysts had a low selectivity towards the products[2] or they were not efficient enough. As can be seen in Figure (2), this process is rather tricky because activating the carbon monoxide implies surpassing the HOMO-LUMO gap[13][14] with light, and carefully selecting what chemical species is desired from CO is one of the biggest challenges with these catalysts. Therefore, one of the main objectives of the scientific community in this field is to improve on these aspects.

In addition to what has been said, AP has also been studied both computationally[13] and experimentally[15][16] on a similar reaction of this work (*vide infra*) with porphyrinic catalysts. All of them

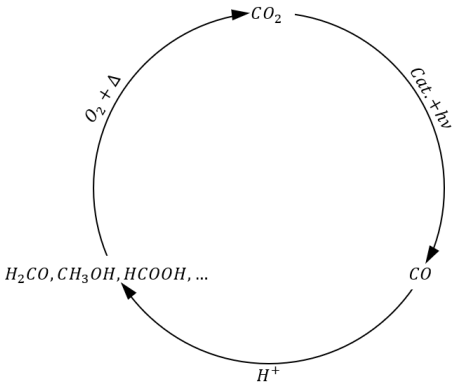

Figure 2: Simplified scheme of the catalytic cycle of the artificial photosynthesis.

concluded that the catalyst's acidic protons are fundamental to obtaining CO and H_2O from CO_2 *via* an acid-carboxylic-like intermediate; this mechanism is called Proton-Assisted Mechanism (PAM). However, there is another mechanism that is not proton assisted and is based on a disproportionation mechanism. A disproportionation is defined as a process in which the substrate is oxidised and reduced simultaneously giving two different products with an even difference of oxidation states. For the tetradentate catalyst aforementioned, this mechanism was postulated by Sergio Fernández and Lloret-Fillol *et al.* in 2019[17]. Precisely, they used the $[^{H,H}\text{Py}^{Me}\text{tacn-Co}^{II}(\text{OTf})_2] \equiv [\text{L}^{N4}\text{Co}^{II}\text{-}(\text{OTf})_2] \equiv \mathbf{1}^H$ that is nucleophilic enough to coordinate with CO_2 and transform it into both CO and carbonate anion.

A problem of CO_2-to-CO catalysis using $\mathbf{1}^H$ is that the $[\text{Co}^I\text{-CO}]$ intermediate formed along the activation of CO_2 after the electrochemical reduction of the catalyst is very stable due to the π back-bonding to the cobalt metallic centre.

$$[L^{N4}Co^{II} - CO]^{+2} \xrightarrow{e^-} [L^{N4}Co^{I} - CO]^{+} \;\; E^0 < 0 \;\text{ and }\; \Delta G^0 < 0 \tag{1}$$

The Co^{II} metallic centre is poor on electrons whereas the Co^I is slightly richer. Moreover, the $[\text{Co}^I\text{-CO}]$ complex stability can also be explained by means of the $18e^-$ counting rule[17].

This fact triggers both the PAM and disproportionation mechanisms to present an energetic well that traps the $[\text{L}^{N4}\text{Co}^I\text{-CO}]^+$ intermediates formed, preventing the reaction to proceed further, without external stimulation, from the first catalytic cycle.

To reduce the potential well (PW) that prevents the reaction to occur catalytically there are two possibilities: the first involves irradiating the system with blue light, which labilises the M-CO bond[18] or, the second, finding an alternative path that prevents the formation of the Co^I species and conserves the Co^{II} species that have a more labile Co-CO bond.

A simplified scheme of the disproportionation mechanism of the CO_2-to-CO reduction catalysed by $\mathbf{1}^H$ is shown in Figure (3).

This work focuses on proposing a strategy to reduce the PW and the energy of the [TS2] of the disproportionation mechanism energy using externally oriented electric fields. The existence of this PW is based on the energetic difference between the most stable species, i.e. [i.10], and the [i.2] intermediate. Computational Chemistry allows the individual study of each species involved in the thermodynamic pathway. In this work, we have studied two different energy differences in order to

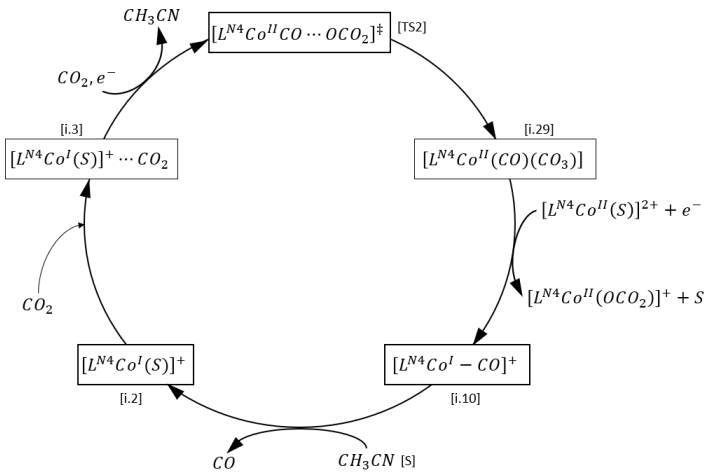

Figure 3: Dismutation mechanism of CO_2 through some of the key intermediates treated in this study. CH_3CN is simplified as S.

rationalise the effect of the electric field on the kinetics of the catalysis: a) The CO release, which is defined explicitly as potential well in Equation (2):

$$[L^{N4}Co^{I} - CO]^{+} + MeCN \rightarrow [L^{N4}Co^{I} - NCMe]^{+} + CO \tag{2}$$

and b) the energy difference between the TOF-determining transition state (TDTS) and the TOF-determining intermediate (TDI, see Section 4.2 for the nomenclature), which determines the TOF of the catalysis as Eq. (3) shows.

$$[L^{N4}Co^{I} - CO]^{+} + 2CO_2 \xrightarrow{e^-} [L^{N4}Co^{II} - CO\cdots OCO_2]^{\ddagger} + CO \tag{3}$$

Studying the PW and TDTS-TDI energies are a good approach to having a good grasp of how the TOF of the catalytic cycle is tuned.

Notice that the chemical transformation of Eq. (3) also includes an ET transfer process, therefore, the whole system must rely on electrocatalysis. A note on the catalyst, $\mathbf{1}^H$ is robust enough to resist reduction potentials of -1.91 V vs $Fc^{0/+}$ without decomposing so one can expect it can work in a wide range of reduction potentials.

Using electric fields (EFs) to induce catalysis is not a recent discovery as it has been used to enhance simple reactions[19] such as Diels-Alder cycloadditions[20], where the EFs may be used to drive the electrons to either enhance, or inhibit, the reaction rate. EFs have also been applied in photo/excited chemistry[21], molecular diads with fullerenes[22], and quantum tunnelling at low temperatures[23], charge transfer processes in excited states[24], to cite several examples.

Sason Shaik and coworkers in parallel with Teresa Head-Gordon *et al.*, in many of their papers, have established the theoretical background of the effect of the EFs on reactivity[25][26][27][28]. In this work, we study the effect of an External Electric Field (EEF) on the CO_2-to-CO reduction catalysed by a Co complex studied by Fernández *et al.*[17]. Specifically, we will focus on the effect of EEFs on the PW and TDTS-TDI.

The FDB_β method is an accurate and cheap method developed in the group[29]. It is MxN-times faster than performing calculations in the presence of explicit electric fields, where M and N are the

number of involved species and explicit field computations, respectively. FDB_β method is based on the subtraction of the Taylor series expansion centred at zero of the field-dependent electronic energies of the transition state (or products) and reactants (see Section 3.2). This model may help both experimental and computational chemists to design catalysts that include charged functional groups that generate internal EFs to improve the efficiency of different catalysis.

2 Objectives

The main objective is to propose a strategy to reduce the PW of the CO_2-to-CO reductive disproportionation mechanism using $\mathbf{1}^H$. Particularly, we aim to offer an approach to reduce the PW and TDTS-TDI energies using externally oriented EFs.

The main goal has been split into several more focused objectives:

1. Characterise using DFT the species that determine the potential well and TDTS-TDI of this mechanism.
2. Assess the impact of an EF on the PW and TDTS-TDI through the FDB_β method on judiciously selected axes.
3. Generalise the previous objective into an arbitrary number of axes.
4. Conceive an approximation to reduce the computational cost of the FDB_β method for bulkier or harder-to-characterise chemical systems.
5. Find the optimal EEF, or the lowest EEF, for a specific target barrier through the development of new software.
6. Study a model-sized system with both explicit fields and point-like charges and compare the results obtained with the FDB_β method. Then export the knowledge extracted to the $\mathbf{1}^H$ catalyst.

3 Theoretical background and computational details

3.1 Computational details

The electronic structure calculations of each species have been carried out using the Gaussian16a03[30] software package and the visualisation of the results *via* the Chemcraft 1.8 software[31]. The before mentioned mechanism has been studied by Density Functional Theory (DFT). More specifically, with the B3LYP[32] hybrid functional with GD_3 empirical dispersion[33] alongside a Self-Consistent Reaction Field (SCRF). The SCRF is based on the SMD model[34] to describe the system in a solution of acetonitrile. Altogether, the full method to solve Schrödinger's-like equations (the Kohn-Sham equations) is the B3LYP-D_3(SMD). For optimisations, the 6-31+G(d) Pople's basis set has been used and a trimmed version of Dunning's basis set aug-cc-pVTZ[35], where one of the diffuse functions with higher angular momentum (quantum number l) has been erased to gain in computational time and still achieve good results, for single point calculations. Thus, the computational level used is the B3LYP-D_3(SMD)/aug(-d^H,-$f^{C,N,O}$,-g^{Co})-cc-pVTZ// B3LYP-D_3(SMD)/6-31+G(d). More in-depth, the first basis set has been used for calculating single point energies and electric molecular properties; the second one for the characterisation of stationary points, both intermediates and transition states (TS), geometry optimisation, computation of analytic harmonic vibrational frequencies, and nuclear relaxation polarizability matrices (*vide infra*) for the bulkiest species. The nature of each stationary point has been determined by the number of imaginary frequencies with an analytic computation of harmonic frequencies, as has been stated just now.

Note that, the basis set used for single point computations is a bit larger than the one used by Sergio *et al.*[17], for that reason, our base is slightly more flexible when computing energies, thus, more accurate results as a consequence of the Variational Theorem. On top of that, Gaussian16 has a smaller default grid than Gaussian09 to calculate the numerical integrals related to DFT, which implies a smaller numerical error associated with the outcome.

The Gibbs free energy has been computed as a correction of the electronic energy. First, the $G_{i,corr}$ obtained with the frequency calculation which includes the thermal and entropic corrections; second, the $RT\ln(24.4c_i)$ term, which describes the Gibbs energy correction associated with the conversion from standard-state gas-phase pressure of 1 atm to the desired concentration in mol/L and. For instance, the standard value of 1M at 298.15K (working temperature) is 1.89 kcal/mol. Therefore, obtaining the following expression for each species that only depends on the experimental concentration:

$$G_i = E_i + G_{i,corr} + RT\ln(24.4c_i) \tag{4}$$

Then, the Gibbs energy of the R $\rightarrow$ P reaction is given by this next expression:

$$\Delta G = \Delta E + \Delta G_{corr} + RT\ln\frac{[P]}{[R]} \tag{5}$$

Where R is the universal gas constant, T is the temperature (K). The last correction is only significant when $[P] \neq [R]$.

For those steps that include ET processes such as reductions or oxidations, the extra energy carried by the electron must be taken into account either in the reactant or product species. On the grounds

that in the original reference, they work at a reduction potential of -1.91 V vs $Fc^{0/+}$ the (free Gibbs) energy of an electron carries must be transformed in the Standard Hydrogen Electrode (SHE) reference frame. This is done in the following manner:

$$E^0(V) = -(\frac{\Delta G^0}{nF} - \frac{\Delta G^0_{SHE}}{F}) - 0.624 \tag{6}$$

Where ΔG^0 is the standard free Gibbs energy, 0.624 is the corrective factor for the ferrocene reference electrode to the SHE in acetonitrile medium, F is the Faraday constant, n is the number of electrons involved in the ET process, $\Delta G^0_{SHE} = -4.28eV$. Reorganising (6) one can find the readjusting factor to include on one species:

$$\Delta G^0 = -nF(E^0(V) + 0.624 - \frac{\Delta G^0_{SHE}}{F})$$

Depending on which molecule of the reaction this correction is added, the sign of the correction must be changed to properly describe the thermodynamics of the system. In the following sections, this factor will not be mentioned yet it is considered for the computation of energies and modelling of the system.

When the effects of explicit homogeneous fields and charges are assessed (see Chapter 5), a different computational methodology is used. Only gas-phase single-point calculations have been performed at the B3LYP-D_3/6-31+G(p,d) level of theory. The additional "p" in the basis set indicates the definition of polarisation functions are also included in the hydrogen, hence, adding extra orbitals with higher angular momentum associated with their respective basis set functions. Only when the reaction mechanism is studied, B3LYP-D_3/aug(-d^H,-$f^{C,N,O}$,-g^{Co})-cc-pVTZ level of theory has been applied to improve the results.

To assess the electrostatics effects caused by the charges for any given molecule, one must take into account the charge of the molecule and the number of point charges used to perform the study. In this work, only up to two charges (**2Q**) aligned on the same axis have been considered. Then, for a neutral molecule, the potential energy correction to the total energy given by Coulomb's Law due to two point charges of different signs placed on the same axis, and at the same distance of the molecule, but on opposite sides is:

$$E_{\mathbf{2Q}} = E_0 + \frac{Q^+Q^-}{2(r/a_0)} \tag{7}$$

where a_0 is Bohr radius, which also acts as the converter from angstroms to atomic units, and E_0 is the field-dependent electronic energy of the molecule.

When the object of study has a non-zero formal charge, it must be also considered the potential caused by the repulsion(attraction) between the molecule and one charge:

$$E_{M\cdots Q} = E_0 + \frac{Q^+_M Q^\pm}{(r/a_0)} \tag{8}$$

where Q^M is the formal charge of the molecule and Q_i refers to the point charges. If two point charges of different signs are placed on the same axis, and at the same distance of the molecule, but on opposite sides, the total energy is given by:

$$E_{Q_i \cdots Q_j} = E_0 + \sum_{i=1}^{2} \frac{Q_M Q_i}{(r/a_0)} + \frac{Q^+ Q^-}{2(r/a_0)} = E_0 + \frac{Q^+ Q^-}{2(r/a_0)} \tag{9}$$

On the same note, the last term is the electrostatic potential generated by both point charges. In this particular case, note that Equations (7) and (9) are analogous due to the cancellation of the second term caused by the interaction of the charged molecule with the two charges of opposite sign. This cancellation is only possible when there is the same number of positive and negative charges, have the same magnitude, and are perfectly aligned on the same axis. Therefore, in this particular case, defining two point-like charges makes no difference to the corrections applied to a charged, or neutral, molecular system. If it were to be studied with non-aligned charges, Equation (9) should be reformulated to reflect the new environment.

3.2 FDB$_\beta$ Code

The method developed by Pau Besalú *et al.* for the *Fast and Simple Evaluation of the Catalysis and Selectivity Induced by External Electric Fields*[29] alows determining the strength and direction of an external electric field that is required to reduce or increase the barrier of a reaction.

FDB$_\beta$ is based on expanding the zero-field energy of a chemical species in a Taylor series in the strength of an electric field.[36][37]:

$$E(\mathbf{F}) = E(0) - \boldsymbol{\mu}\mathbf{F} - \frac{1}{2!}\boldsymbol{\alpha}\mathbf{F}^2 - \frac{1}{3!}\boldsymbol{\beta}\mathbf{F}^3 - \frac{1}{4!}\boldsymbol{\gamma}\mathbf{F}^4 + \dots \tag{10}$$

Where $\boldsymbol{\mu}$, $\boldsymbol{\alpha}$, $\boldsymbol{\beta}$ and $\boldsymbol{\gamma}$ are the expansion coefficients corresponding to the dipole moment, electric polarizability, and the first and second-order hyperpolarizability tensors, respectively. Then, the activation energy/thermochemistry of a reaction, and in general, any energy change is given by the difference of the Taylor expansions of TS/products and the reactants, and their electric properties ($\mathbf{P}$):

$$\Delta E^{\ddagger}(\mathbf{F}) = E_{TS}(\mathbf{F}) - E_R(\mathbf{F}) \qquad \Delta \mathbf{P}^{\ddagger}(\mathbf{F}) = \mathbf{P}_{TS}(\mathbf{F}) - \mathbf{P}_R(\mathbf{F}), \forall \boldsymbol{P} = \boldsymbol{\mu}, \boldsymbol{\alpha}, \boldsymbol{\beta}, \boldsymbol{\gamma}, ... \tag{11}$$

$$\Delta E(\mathbf{F}) = \Delta E(0) - \Delta\boldsymbol{\mu}\mathbf{F} - \frac{1}{2!}\Delta\boldsymbol{\alpha}\mathbf{F}^2 - \Delta\frac{1}{3!}\boldsymbol{\beta}\mathbf{F}^3 - \Delta\frac{1}{4!}\Delta\boldsymbol{\gamma}\mathbf{F}^4 + \dots \tag{12}$$

On top of that, as it has been demonstrated in the original work with a Diels-Alder reaction with four possible products, the stereoselectivity of a reaction can also be regulated using EEFs[28][29]. In general, this method of calculating energetic and property differences comes with a low computational cost simply because one only has to calculate the energy and electric properties of two compounds and if there are not any secondary species involved, with only a single computation per molecule. In other words, this approach does not require the calculation of the chemical systems with explicit electric fields.

A general procedure simply involves an *opt freq* calculation for each species without explicit field, that is, at free-field. Using the *freq* keyword already comes with several benefits: characterisation of the stationary point, determination of several NLOP[2](dipole moment and polarizability) and the α_{NR}

[2]The keyword *Polar* is done by default when second derivatives are computed analytically. `https://gaussian.com/polar/`

(*vide infra*). Then, it is only followed by subtraction of the energies and properties as it is shown in Equations (11) and (12).

To correctly compute the NLOPs of a charged chemical species, the electronic structure must be defined referencing the centre of charge. This last concept is analogous to the centre of mass:

$$\boldsymbol{\mu}_Q = \frac{1}{Z_T} \sum_{i=1}^{N_{atoms}} Z_i r_i \quad \text{where} \quad Z_T = \sum_{i=1}^{N_{atoms}} Z_i \tag{13}$$

They must be computed in that manner because the dipole moment and first hyperpolarizability of a charged molecule are origin-dependent properties[38][39], and consequently, they require a reference frame to be properly compared.

Although the method is computationally very efficient, there was missing a tool to automatically determine the required EF to tune any given barrier. This gets even more complicated when there are several EEF acting on the catalysis. With the help of Pau Besalú, we have developed a FORTRAN95 code that can find the minimum strength of EF associated with a targeted barrier by solving the equation (12) iteratively.
The functionality of the code is based on three considerations:

1. Beta approximation: on the grounds that calculating the gamma coefficient is computationally expensive, due to it being the fourth derivative with respect to electric field of the field-dependent electronic energy[40], and the results up to the third order term are already quite accurate, the code works with the truncation up until the beta coefficient.

2. Effect of the vibrational polarizability: EFs induce changes in the equilibrium geometry and the relaxation of the electronic structure provoked by the perturbation is reflected in the nuclear relaxation (NR)[41]. The isotropic polarizability can be split into three main terms but only two of them are relevant in this study:[42]

$$\alpha(\mathbf{F}) = \alpha^{el} + \alpha^{NR} + \alpha^{curv} \approx \alpha^{el} + \alpha^{NR} \tag{14}$$

   Therefore, on top of the α_{el}, the nuclear relaxation polarizability matrix(α_{NR}) has also been considered. Notice that the hyperpolarizabilities have also vibrational contributions, however, they have not been calculated.

3. Redox reactions: for cases in which there is involved either a reduction or an oxidation, it has been implemented an internal keyword that determines the reduction potential(vs SHE) and adds the energy to the reactant species to consider this extra energy that carries the electron.

From the input file, it generates the necessary set of algebraic objects (vectors, matrices, and tensors) that describes the studied system. Out of the same file, it is also taken the maximum strength of the electric field that one wants to be examined. Intrinsically, it is being generated a cube of side $2 \cdot F_{max}$ which contains a sphere of radius F_{max}:

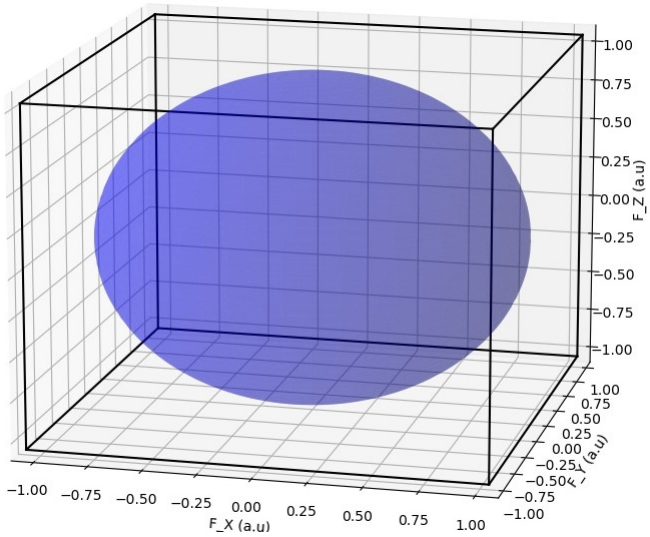

Figure 4: Visual conceptualisation of the scanning procedure of the FDB$_\beta$ code

On one hand, inside the cube represent all the strengths and directions of EFs considered. On the other hand, the blue sphere in Figure (4) contains the values of ΔG that can reach with an EEF of maximum modulus 0.01 a.u. Additionally, inside the latter is where it will be done the search for the optimal EEF for the specified target barrier. Once the background of the program is known, its operation is rather straightforward (see Figure (5)).

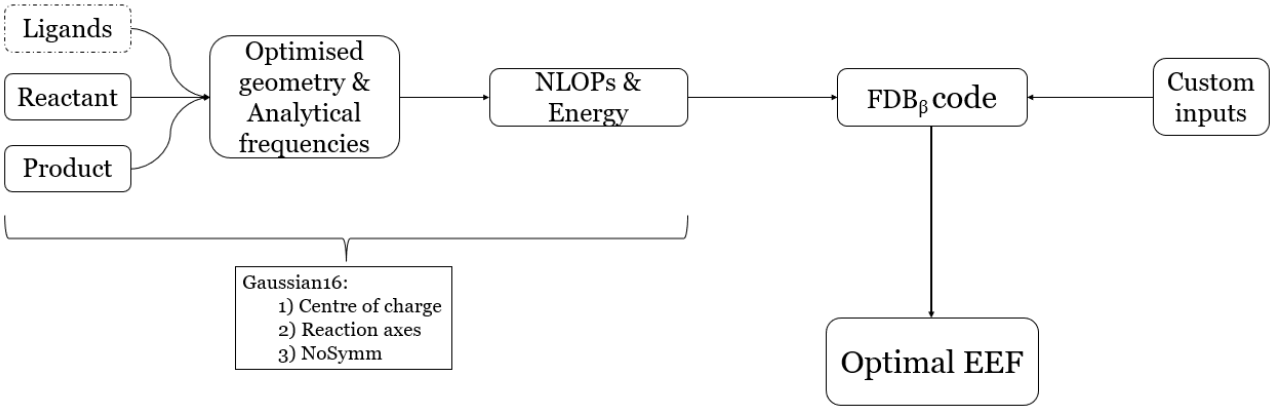

Figure 5: Flowchart of the operation of the FDB$_\beta$ code to obtain the optimal EEF for a certain barrier.

To properly portray the data it is mandatory to use a scatter graph with only markers because Equation (12) is not a unique function. In other words, the same value of ΔG can be achieved by different field values.

If the reader would like to read more about the program, more information can be found in `https://github.com/imGuillem/3D-FDB_Beta.git`.

3.3 ProfilE software

Besides the creation of the FDB$_\beta$ code, the use of a code created in the IQCC and ICIQ has been crucial for the development of this work, not only for its intended function but to also confirm the results obtained from the previous section.

ProfilE is a Visual Basic-based software coded in ICIQ and IQCC that uses an Excel sheet as input with the purpose of not only generating reaction profiles but also exploring the effect of the reduction potential (vs SHE), pH, and electric field($\cdot 10^4$ a.u) in the profiles. Together with a Python script, one can generate 2-D diagrams like the ones that appear in the works of Besalú *et al.*[29] or Fernández and coworkers[17], among other functionalities.

As a consequence of how this code is programmed, one cannot study reactions that have more than one step and they should be split into its elementary steps.

For instance, the non-elementary reaction:

$$A + B \rightarrow C + D$$

must be split into its elementary steps:

$$A + B \rightarrow X + D \rightarrow C + D$$

where X is an intermediate.

For the cases where there is an ET process, they must be also included as elementary steps. For example, the thermodynamic cycle decomposition of the reaction $[i.10] \rightarrow [TS2]$ of Figure (3):

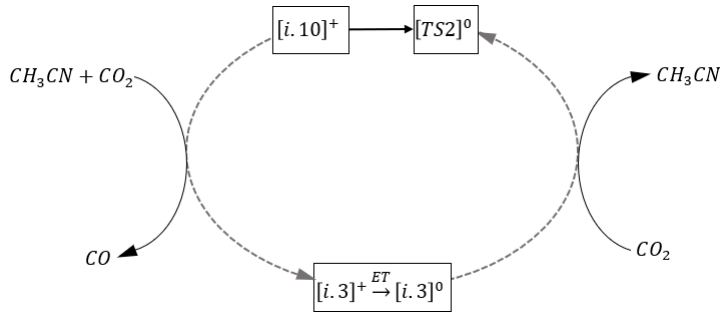

Figure 6: Reaction pathway of the transition of [i.10] to [TS2] within the mechanism proposed by Fernández *et al.*

This mechanism will later be studied in the following chapter.

Besides this "setback", ProfilE is a powerful tool that has taken a major role in this work by both giving results, portraying them, and helping confirm some others.

4 Aprotic mechanism. Computational study with the FDB$_\beta$ method

4.1 Study of the Potential Well

To study the effect of the EEFs on the potential well it is capital to define thoroughly the Cartesian axes used to define the vector field ($\vec{F}$) orientation (See Fig. (7)).

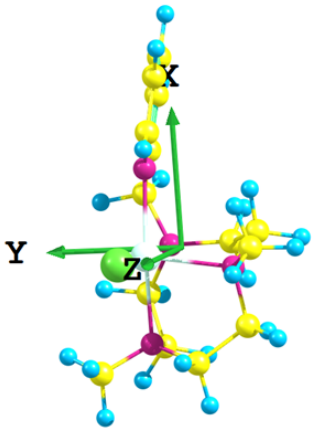

Figure 7: [L$_{N4}$Co-L'] catalyst. The green sphere represents either CO or MeCN, or a ligand in general

The centre of the vector field, for any species in this work, is defined at the centre of charge (*vide supra*). Then, the axes are set to go from the centre to the pyridine (X), to the coordination vacant (Y) and to the CO/MeCN ligand (Z). The Z axis is also defined as the principal reaction axis where the CO-CH_3CN ligand exchange is going to occur.

Furthermore, something else must be taken into consideration namely how Gaussian defines the electric fields[25]. The so-called physical convention is to define them as a vector from the positive charge source towards the negative charge, however, Gaussian16 defines it the other way around: from negative to positive sign of the Cartesian axis. Unless it is mentioned, this work will follow the physical convention to avoid inconsistencies.

First, we will study how the EFs simulated by the FDB$_\beta$ method can help to reduce the potential well formed by the difference of the energy of the [i.10] and [i.2] species (See Figure (8)). For simplicity, from now on, the PW will be interchangeably named "CO release" or simply "Release".

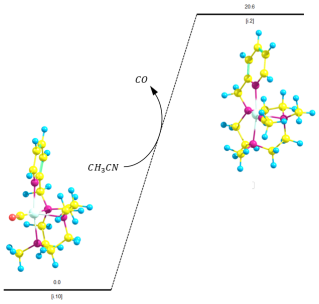

$$\longleftrightarrow \qquad [i.10] + CH_3CN \rightarrow [i.2] + CO$$

Figure 8: [i.10] to [i.2] (CO Release) due to an exchange of ligands.

Then, the energy balance of the reaction is expressed by the subtraction of Taylor series expansions considering the thermochemistry of the process:

$$E_{RLS}(\boldsymbol{F}) = E_{[i.2]}(\boldsymbol{F}) - E_{[i.10]}(\boldsymbol{F}) + E_{[CO]}(\boldsymbol{F}) - E_{[CH_3CN]}(\boldsymbol{F}) \tag{15}$$

In order to include the perturbation of the EEFs, one must use the Equation (12). When EEFs are applied to the reaction, it is considered that it also affects the molecules of solvent (MeCN) and CO and that they have the freedom to orient their dipole moment with the EEF. This comes with a consequent stabilisation, independent of the orientation of the EEF, applied to the intermediates. Therefore, the positive and negative fields of the same magnitude have the same stabilising effect on CH_3CN and CO molecules.

In Figure (9), we show the 1-D profiles of the effect of the EEF on the CO release obtained using the FDB_β code.

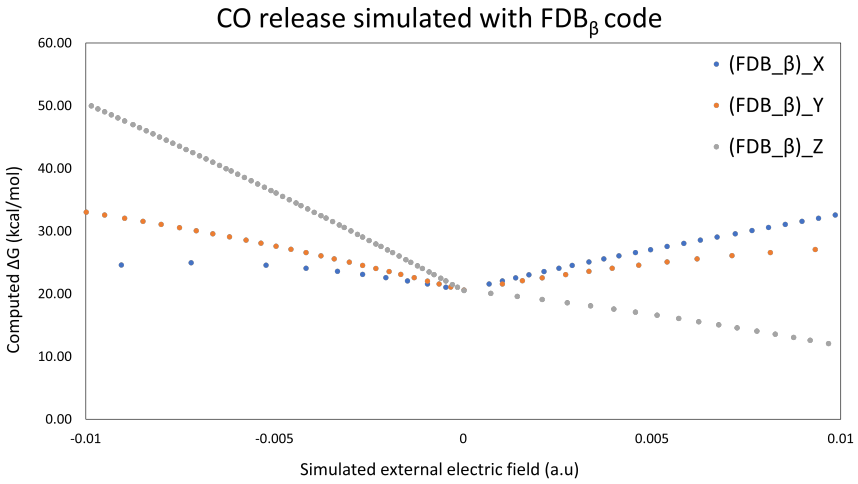

Figure 9: ΔG values of the CO release obtained through the FDB_β method implemented in a FORTRAN95 code.

As can be seen in Figure (9) the Z axis is the most relevant reaction axis and the application of an EFF in this axis is responsible for reducing the most the CO release. Considering the free-field value of 20.56 kcal/mol, applying an EEF in the Z-axis can increase the energetic difference of the potential well up to 50.40 kcal/mol (F_Z=-0.01 a.u) or decrease it down to 11.73 kcal/mol (F_Z=0.01 a.u). Therefore, the studied strengths of the electric field may induce a variation range of 38.67 kcal/mol. On the other hand, applying an EEF in the X axis diminishes the PW to 24.14 kcal/mol (F_X=-0.01 a.u) and increases it to 32.76 kcal/mol (F_X=0.01 a.u), whereas applying an electric field in the Y axis induce a change in the PW from 33.03 kcal/mol (F_Y=-0.01 a.u) to 27.36 kcal/mol (F_Y=0.01 a.u) with an overall variation range of -8.63 and 5.66 kcal/mol, respectively. Therefore, the X and Y axes have a minor role in hindering the CO release, and then, they induce the opposite change in the PW of what wants to be achieved in this work.

As it is illustrated in Figure (10), the significant relevance of the Z-axis stems from its alignment with the Co-CO axes of the molecular structure of [i.10], which of course it is the most important axis in the release of the CO. In contrast, the X axis corresponds to the Co-pyridine axis which as may be expected has a less important role in the CO release. The same is true for the Y axis. Therefore, applying an EF in the direction of the [Co-CO] bond can induce the cleavage of the bond between the Co and CO. And then, as the equation in Figure (8) indicates, it will be followed by the entrance of a CH_3CN molecule coming from the solvent bulk, and then restarting the catalytic cycle.

To carry on with the study of the release system, we also studied the effect of applying an EEF

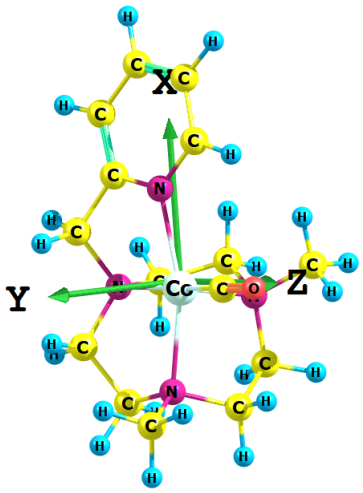

Figure 10: [i.10] molecular structure with the atoms labelled together with Cartesian axes.

in any direction of a plane. Diagrams such as (11) are generated not only to confirm the results of the Figure (9) but also to have a good grasp on how the ligand exchange behaves when there are EEFs. For this type 2-D plots, constant values of field-dependent ΔG are presented as dotted lines (i.e. isoenergetic curves).

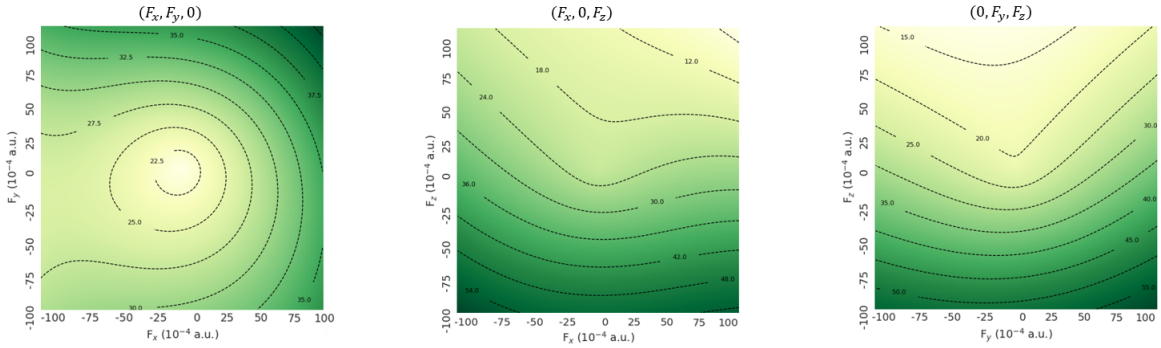

Figure 11: 2-D diagrams of the effect of two different electric fields (F_i,F_j) on the release barrier with a constant third field (F_k=0 a.u)

In the left 2D-diagram of Fig. (11) is shown the effect on the release barrier of applying any (F_X,F_Y) EFs with a constant F_Z=0 a.u. This figure also illustrates that applying EFs in the X and Y axes does not induce large changes in the thermodynamics of the PW, since the maximum change in the chemical barrier for the F_X and F_Y scanned is less than 10 kcal/mol while applying an F_Z triggers a change of almost 40 kcal/mol.

On the contrary, scanning the effect of the (F_X,F_Z) EFs on the release barrier with a constant F_Y=0 a.u manifests, that only the field vector F_Z can trigger a reduction in the release barrier up to 12 kcal/mol. Considering extremely positive field values of F_X there is a minor diminishing effect. Nonetheless, they are non-achievable experimental fields.

Last but not least, scanning the effect of the (F_Y,F_Z) EFs on the release barrier with a constant F_X=0 a.u shows again that the field in the Z-axis has a major role in favouring/hampering the CO release. This 2-D graph shows explicitly the invariability of CO release Gibbs energy with respect to the strength of the Y-axis electric field.

Thereafter, exclusively with the information within these diagrams, without any further knowledge of the system, one can make solid predictions about the effect of the electric field on the reaction. Furthermore, to design a more efficient catalyst, it is better to work on (F_X,F_Z) field vectors (see central 2D-diagram of Figure (11), although the major change is clearly given by the F_Z component.

Now, if, for instance, we fix the F_Z=±0.005 a.u and scan through the (F_X,F_Y) EFs it is obtained the following set of diagrams in Figure (12).

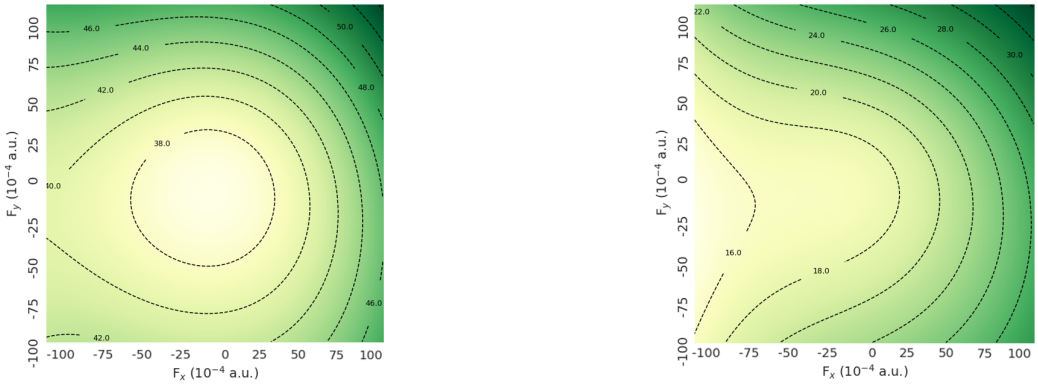

Figure 12: Scan of the (F_X,F_Y) electric fields with the effect of a constant F_Z=-0.005a.u (left) and 0.005a.u (right)

What is interesting about Figure (12) is the abrupt change in the topology of the (F_X,F_Y) scan with the different constant values of F_Z. This variation directly suggests the question of whether a three-dimensional vector field is a possibility to reduce the potential well. On the contrary, the other two possible sets of scans, i.e. fixing a constant value of F_X or F_Y, do not give new insightful information.

As has been stated in the previous chapter, finding the optimal EEF (OpEEF) for a certain value of the barrier is not a trivial task; it can be done by analysing the results with the 2-D diagrams, but it is not easy. Then, we implemented in the FDB$_\beta$ code an algorithm to determine which strength and directions of the electric field give a specific barrier scanning a radius of 0.01 atomic units.

For example, to achieve a barrier of ∼12 kcal/mol, while considering a maximum discrepancy of 0.1 kcal/mol, the ten first lines of the output of the code for the possible EEFs are the following:

$$\vec{F} = (-83.99, 0.22, 54.01) \cdot 10^{-4} a.u \quad |F| = 99.9 \cdot 10^{-4} a.u \quad \Delta G(\text{kcal/mol}) = 12.10$$
$$\vec{F} = (-83.99, 13.36, 53.13) \cdot 10^{-4} a.u \quad |F| = 99.9 \cdot 10^{-4} a.u \quad \Delta G(\text{kcal/mol}) = 12.08$$
$$\vec{F} = (-83.55, -2.425, 54.89) \cdot 10^{-4} a.u \quad |F| = 100.0 \cdot 10^{-4} a.u \quad \Delta G(\text{kcal/mol}) = 12.02$$
$$\vec{F} = (-83.55, 7.715, 53.57) \cdot 10^{-4} a.u \quad |F| = 99.5 \cdot 10^{-4} a.u \quad \Delta G(\text{kcal/mol}) = 12.08$$
$$\vec{F} = (-83.11, -5.511, 55.33) \cdot 10^{-4} a.u \quad |F| = 100.0 \cdot 10^{-4} a.u \quad \Delta G(\text{kcal/mol}) = 12.05$$
$$\vec{F} = (-83.11, 4.629, 54.01) \cdot 10^{-4} a.u \quad |F| = 99.2 \cdot 10^{-4} a.u \quad \Delta G(\text{kcal/mol}) = 12.09$$
$$\vec{F} = (-83.11, 14.77, 53.57) \cdot 10^{-4} a.u \quad |F| = 100.0 \cdot 10^{-4} a.u \quad \Delta G(\text{kcal/mol}) = 12.00$$
$$\vec{F} = (-82.67, -7.275, 55.77) \cdot 10^{-4} a.u \quad |F| = 100.0 \cdot 10^{-4} a.u \quad \Delta G(\text{kcal/mol}) = 12.04$$
$$\vec{F} = (-82.67, 2.866, 54.45) \cdot 10^{-4} a.u \quad |F| = 99.0 \cdot 10^{-4} a.u \quad \Delta G(\text{kcal/mol}) = 12.08$$
$$\vec{F} = (-82.67, 13.01, 53.57) \cdot 10^{-4} a.u \quad |F| = 99.4 \cdot 10^{-4} a.u \quad \Delta G(\text{kcal/mol}) = 12.08$$

and the last ten lines of the output:

$$\vec{F} = (4.19, 7.275, 98.54) \cdot 10^{-4} a.u \quad |F| = 98.9 \cdot 10^{-4} a.u \quad \Delta G(\text{kcal/mol}) = 12.05$$
$$\vec{F} = (4.19, 17.41, 97.21) \cdot 10^{-4} a.u \quad |F| = 98.9 \cdot 10^{-4} a.u \quad \Delta G(\text{kcal/mol}) = 12.09$$
$$\vec{F} = (4.63, -1.54, 99.86) \cdot 10^{-4} a.u \quad |F| = 100.0 \cdot 10^{-4} a.u \quad \Delta G(\text{kcal/mol}) = 12.09$$
$$\vec{F} = (4.63, 8.60, 98.54) \cdot 10^{-4} a.u \quad |F| = 99.0 \cdot 10^{-4} a.u \quad \Delta G(\text{kcal/mol}) = 12.07$$
$$\vec{F} = (4.63, 18.74, 97.66) \cdot 10^{-4} a.u \quad |F| = 99.5 \cdot 10^{-4} a.u \quad \Delta G(\text{kcal/mol}) = 12.07$$
$$\vec{F} = (5.07, 0.22, 99.86) \cdot 10^{-4} a.u \quad |F| = 100.0 \cdot 10^{-4} a.u \quad \Delta G(\text{kcal/mol}) = 12.09$$
$$\vec{F} = (5.07, 10.36, 98.54) \cdot 10^{-4} a.u \quad |F| = 99.2 \cdot 10^{-4} a.u \quad \Delta G(\text{kcal/mol}) = 12.08$$
$$\vec{F} = (5.07, 20.50, 97.66) \cdot 10^{-4} a.u \quad |F| = 99.9 \cdot 10^{-4} a.u \quad \Delta G(\text{kcal/mol}) = 12.09$$
$$\vec{F} = (5.51, 4.63, 99.42) \cdot 10^{-4} a.u \quad |F| = 99.7 \cdot 10^{-4} a.u \quad \Delta G(\text{kcal/mol}) = 12.10$$
$$\vec{F} = (5.51, 14.77, 98.54) \cdot 10^{-4} a.u \quad |F| = 99.8 \cdot 10^{-4} a.u \quad \Delta G(\text{kcal/mol}) = 12.07$$

The number of non-optimal field printed by the code may be controlled by a threshold that determines whether two solutions are close enough to be considered as unique, to then omit solutions and give a set of representative points as an output. Specifically, the threshold is calculated as a percentage of the scanning radius, which increases every time the script surpasses it.

The smallest module of the EEF required to achieve a barrier of ∼12 kcal/mol, the OpEEF, found by the code is:

$$\vec{F} = (-35.05, 6.83, 75.17) \cdot 10^{-4} a.u \quad |F| = 83.2 \cdot 10^{-4} a.u \quad \Delta G(\text{kcal/mol}) = 12.10$$

Remark on the output each component of the vector field $\vec{F}$ is different to each others, therefore this output has been obtained using the 3D mode of the FDB$_\beta$ code.

For a grid of 500 points for each axis ($125 \cdot 10^6$ points evaluated), it takes less than 50 seconds to give an output; and for a grid of 250 points ($15.626 \cdot 10^6$ points evaluated), less than 6 seconds. The calculation of the OpEEF for a desired target barrier only requires the optimisation of the field-free geometry of the species involved in the mechanistic step studied and the calculation of their NLOPs (see Figure (5)). In contrast, performing calculations with explicit EFs, which will later be discussed, requires the same amount of free-field calculations and $(4 + 2M)N$ field-dependent computations, where M is the number of ligands involved in the reaction and N is the number of selected positive and negative EEF strengths.

4.2 Study of the TDTS-TDI energy difference

Before moving forward, we want to explain how to determine the kinetics of a catalytic cycle from the Gibbs energy profile of the mechanism. To do so, Sebastian Kozuch and Sason Shaik deduced from a more complex expression the following set of equations to define the kinetic energy barrier of a catalytic cycle[43]:

$$\delta E_{span} = \begin{cases} E_{TDTS} - E_{TDI} & \text{TDTS after TDI} \\ E_{TDTS} - E_{TDI} + \Delta E_r & \text{TDTS before TDI} \end{cases} \tag{16}$$

where TDTS is the Turnover-Frequency(TOF) Determining Transition State, TDI the TOF Determining Intermediate, and ΔE_r is the thermodynamic energy difference between the final reactants and initial products, i.e. the reaction energy. The TDTS-TDI are the TS and the intermediate that maximises the energetic span within the cyclic constraints according to the previous equation.

Then, to determine the kinetics of one catalytic reaction is necessary to calculate the Gibbs energy difference from the TDI to TDTS, i.e. for the studied mechanism from [i.10] to [TS2]. As was explained in the previous chapter, the ProfilE software can deal with elementary mechanistic steps. Therefore, the process from [i.10] and [TS2]must be divided into elementary steps that ProfilE code can handle:

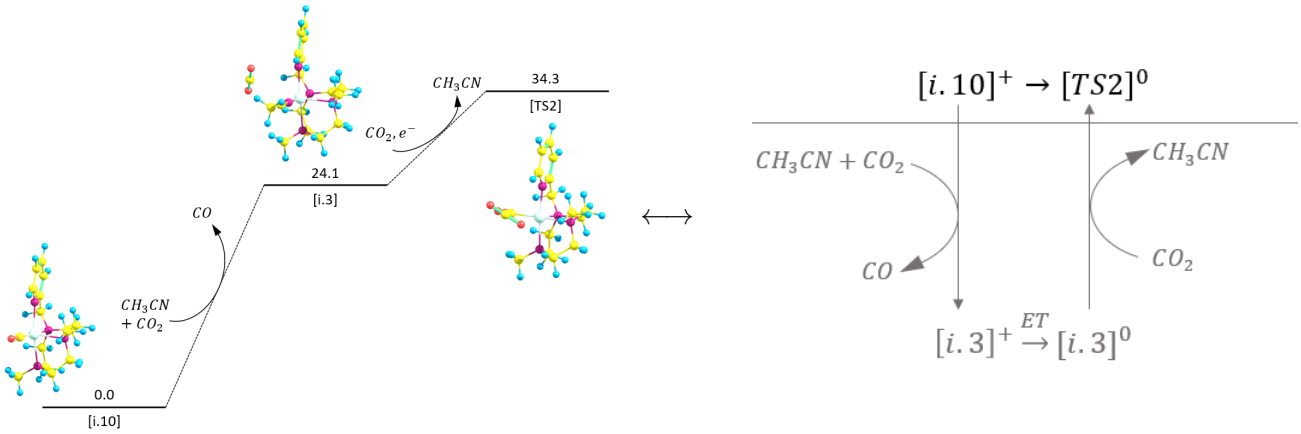

Figure 13: Reaction pathway of the TDTS-TDI transition (left) and the thermodynamic cycle used for its modelling in ProfilE (right).

On the right-hand side of Figure (13), the inked-black reaction is the one that wants to be studied while the grey part is the elementary steps that had to be considered to be able to simulate the system with ProfilE.

Similarly to what has been done in the previous section, the 1-D chart represented in Figure (14) has been computed with the FDB$_\beta$ code.

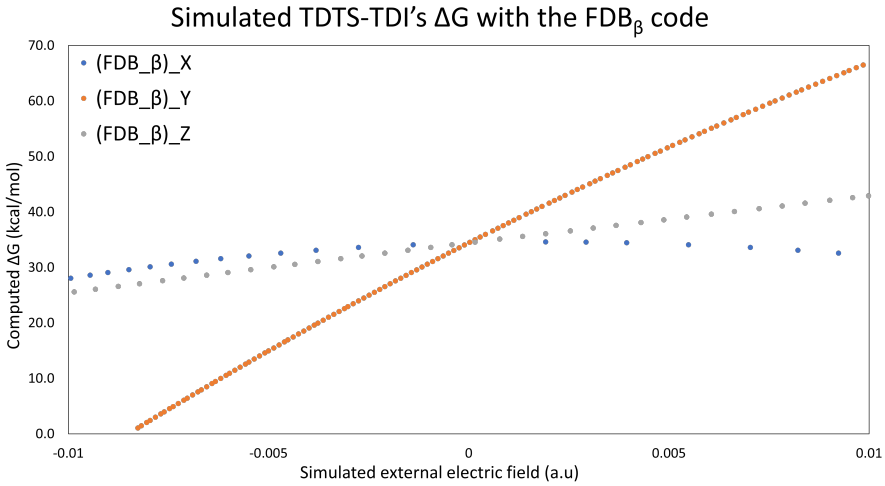

Figure 14: ΔG values of the TDTS-TDI transition computed with the FDB$_\beta$ method implemented in a FORTRAN95 code.

Even though formally the reaction could reach negative barriers when a field is applied in the Y-axis, they are not depicted in the graph since they clearly correspond to non-physical kinetic barriers.

The Figure (14) clearly shows that the application of an electric field in the Y axis has the biggest contribution in controlling the reactivity of $\mathbf{1}^H$, having an energetic variation of 66.80 kcal/mol, ranging from ∼0 kcal/mol (F_Y=-0.01 a.u) to 66.80 kcal/mol (F_Y=0.01 a.u). In contrast, the application of an EEF in the Z-axis has a secondary role in the reactivity, ranging from 25.30 kcal/mol (F_Z=-0.01 a.u) to 42.80 kcal/mol (F_Z=0.01 a.u). The swap of roles of the different fields with respect to the CO release can be justified by looking at the structure of the TDTS.

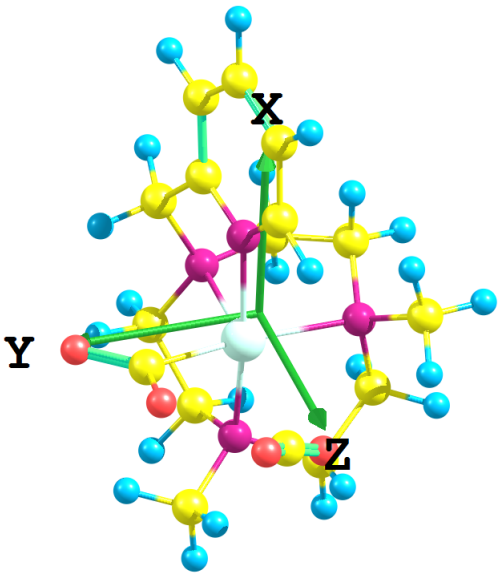

Figure 15: Second transition state corresponding to the formation of the new $Co\cdots CO_2$ bond

This TS is characterised by the formation of a new $Co\cdots CO_2$ bond in the Y axis which generates a high dipole moment on the Y coordinate, explaining the high effect of the EEF applied in this axis to the TDTS-TDI energy. On the other hand, the effect of the EFF on the Z axis is also important because it is where is placed the other $Co\cdots CO_2$ bond. In later steps, in the Y and Z axes are generated the two products of the dismutation: the CO and the CO_3^{2-}, both coordinated to the Co^{II} metallic centre.

It is interesting to note for the TDTS-TDI energy the orientation of the Z-axis EEF that reduces the energy difference is opposite to the one seen in Figure (9). This sudden change is caused by a change of sign in the Z component of [TS2]'s electric dipole moment vector with respect to [i.10]'s counterpart.

Similarly to the previous section, this step of the mechanism has also been studied with the ProfilE software and the subsequent 2-D diagrams have been obtained (see Fig. (16))

Scanning through the (F_X,F_Y) EFs while keeping F_Z=0 a.u confirms that the application of an EEF in the x axis has an almost negligible effect on the TDTS-TDI process, and then in the reactivity of $\mathbf{1}^H$. A similar conclusion can be extracted from scanning through the (F_x,F_Z) EFs while keeping F_y=0 a.u. Then, the most important effect on the energy spam of the studied mechanism are given by the F_y and F_z, although as it can be seen scanning through the (F_Y,F_Z) EFs while keeping F_X=0 a.u, by far the biggest effect is determined by F_y. The (F_Y,F_Z) scan is particularly handy because it combines the two fields that have a major role in perturbing the energy spam of the studied catalysis.

To round up the study in the same fashion as the previous one, we have also used the FDB_β code to determine which EEFs are necessary to reduce the barrier to 12 kcal/mol. The first five lines of

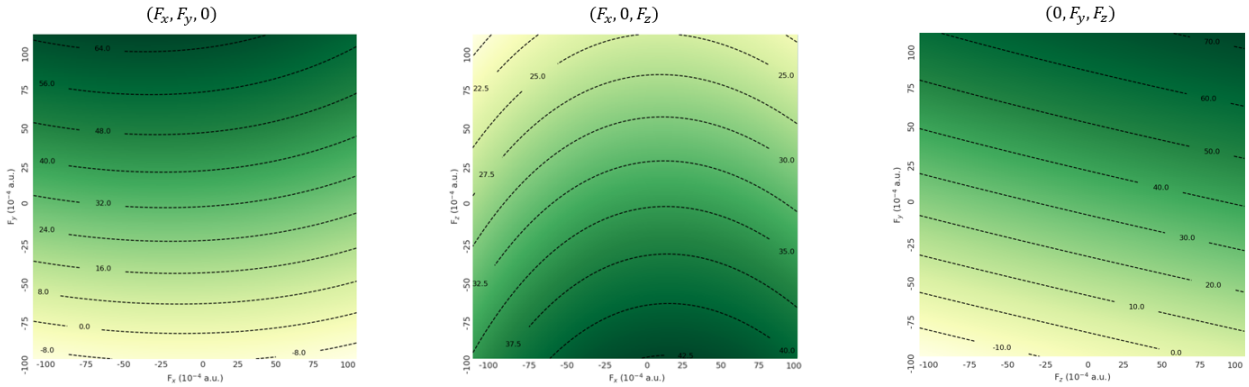

Figure 16: 2-D diagrams of the effect of two different electric fields (F_i,F_j) on the kinetic barrier with a constant third field.

the output for the possible EEFs are the following:

$$\vec{F} = (-89.28, -44.75, -5.070) \cdot 10^{-4} a.u \quad |F| = 100.0 \cdot 10^{-4} a.u \quad \Delta G(\text{kcal/mol}) = 12.05$$
$$\vec{F} = (-39.02, -34.61, -85.31) \cdot 10^{-4} a.u \quad |F| = 100.0 \cdot 10^{-4} a.u \quad \Delta G(\text{kcal/mol}) = 12.04$$
$$\vec{F} = (-80.46, -54.01, 24.47) \cdot 10^{-4} a.u \quad |F| = 99.9 \cdot 10^{-4} a.u \quad \Delta G(\text{kcal/mol}) = 11.93$$
$$\vec{F} = (-38.58, -41.66, -56.21) \cdot 10^{-4} a.u \quad |F| = 79.9 \cdot 10^{-4} a.u \quad \Delta G(\text{kcal/mol}) = 11.94$$
$$\vec{F} = (-88.40, -41.22, -21.82) \cdot 10^{-4} a.u \quad |F| = 99.9 \cdot 10^{-4} a.u \quad \Delta G(\text{kcal/mol}) = 11.97$$

and the last five lines of the output:

$$\vec{F} = (-57.54, -44.75, -32.40) \cdot 10^{-4} a.u \quad |F| = 79.8 \cdot 10^{-4} a.u \quad \Delta G(\text{kcal/mol}) = 11.95$$
$$\vec{F} = (-35.93, -69.44, 60.62) \cdot 10^{-4} a.u \quad |F| = 98.9 \cdot 10^{-4} a.u \quad \Delta G(\text{kcal/mol}) = 11.96$$
$$\vec{F} = (-57.54, -39.90, -53.13) \cdot 10^{-4} a.u \quad |F| = 87.9 \cdot 10^{-4} a.u \quad \Delta G(\text{kcal/mol}) = 11.96$$
$$\vec{F} = (38.14, -52.24, -19.18) \cdot 10^{-4} a.u \quad |F| = 67.5 \cdot 10^{-4} a.u \quad \Delta G(\text{kcal/mol}) = 11.98$$

Then, the OpEEF, that is the EEF with the minimum strength necessary to achieve a barrier of ∼12 kcal/mol found by the code is:

$$\vec{F} = (-2.87, -54.01, -12.12) \cdot 10^{-4} a.u \quad |F| = 55.4 \cdot 10^{-4} a.u \quad \Delta G(\text{kcal/mol}) = 12.10$$

As expected, the largest component is given by F_Y.

5 Effect of charges and explicit fields on the reaction

The goal of this chapter is to compare the results obtained imposing an explicit homogeneous electric field and explicit point charges with the predictions obtained with the FDB$_\beta$ code. First, model systems will be studied. Afterwards, using what has been learnt with the model-sized systems, the equivalent comparison will be done for the studied catalytic mechanism. For simplicity, only the CO release will only be considered.

5.1 H_2O and $[H_2O]^+$ systems

One simple transformation used as a model-sized system is the bending of the water from its angular geometry to the linear shape.

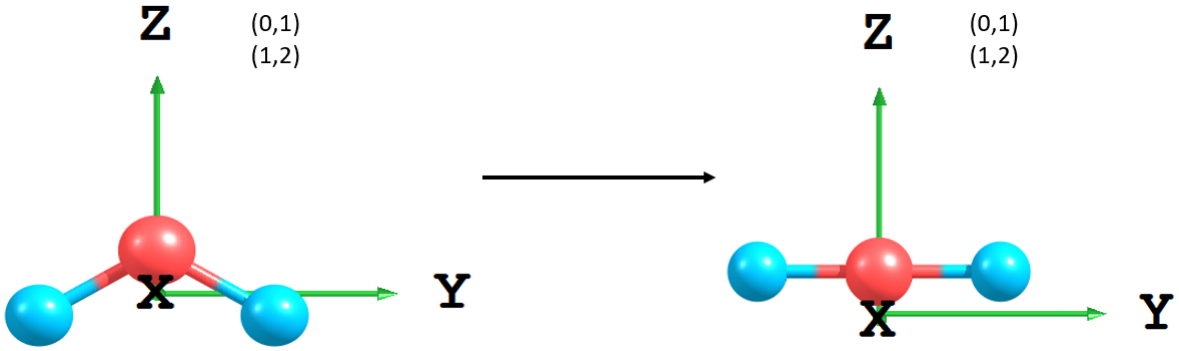

Figure 17: The two geometries of water used as a model-sized system for the comparison of the effect of homogeneous electric fields and point charges with the predictions obtained with the FDB$_\beta$ code. Values in parentheses represent the charge and multiplicity of water molecule, respectively, that have been studied.

The main goal behind the study of the model is to understand better the effects of the fields predicted with FDB$_\beta$, explicit EFs, and point charges, for charged chemical systems, as [i.10] and [i.2]. For example, it is important to understand how to deal with the origin-dependency problems arising from the electrical properties of charged species.

One and two point-charges values have been tested for both systems using different relative positions according to the following nomenclature.

$$Q_{bottom} \equiv \text{Point charge located at Z<0} \qquad Q_{top} \equiv \text{Point charge located at Z>0}$$

$$Q^{-1} \rightarrow Q^{+1} \equiv \text{Negative charge on top and positive charge on the bottom}$$

$$Q^{+1} \rightarrow Q^{-1} \equiv \text{Positive charge on top and negative charge on the bottom}$$

A more schematic way to see this nomenclature is shown in Figure (18).

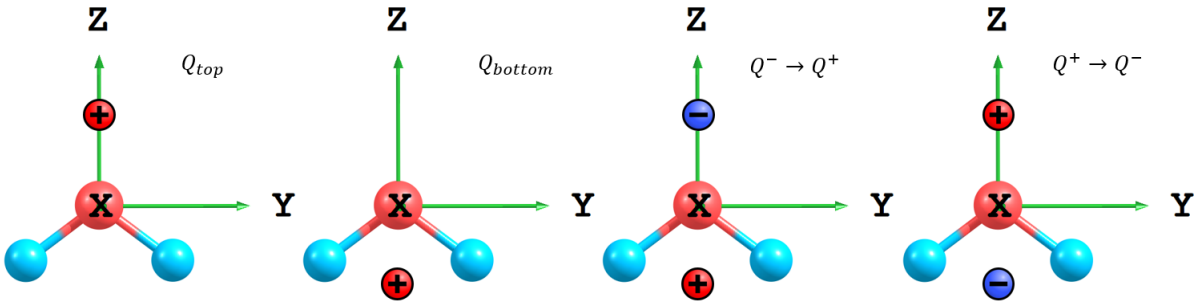

Figure 18: Representative scheme of the charge notation used in this section.

The convention for the electric field sign is the physical convention, hence opposite to the one Gaussian16 uses[25]. Under this nomenclature, Table 1 below shows the results of the change of the energy between the two geometries shown in Figure (17).

Table 1: Energetic difference for the two water geometries (ΔE) shown in Figure (17) using Q=±1 point-charges, explicit homogeneous EFs and FDB$_\beta$ method computed with the 6-31+G(d) basis set. ΔΔE is the energy difference with respect to the fourth and fifth column, respectively. Energies, in kcal/mol, already corrected according to section 3.1 of the Methodology.

	$[H_2O]^0$ **study with Q=±1**											
	Explicit fields using G16			**FDB$_\beta$**		**Point charges**					
	F$_Z$=0	**F$_Z$=-50**	**F$_Z$=+50**	**F$_Z$=-50**	**F$_Z$=50**	**Q$^+_{top}$**	**Q$^+_{bottom}$**	**Q$^-_{top}$**	**Q$^-_{bottom}$**	**Q^{-1}→Q^{+1}**	**Q^{+1}→Q^{-1}**
ΔE(kcal/mol)	25.9954	28.4271	23.5545	28.4271	23.5545	28.0580	23.2420	23.9200	28.7389	23.5679	28.4129
ΔΔE(kcal/mol)	-	-	-	0.0000	0.0000	0.3691	0.3125	-0.3655	-0.3118	-0.0134	0.0142
	$[H_2O]^+$ **study with Q=±1**										
ΔE(kcal/mol)	19.4525	22.3487	16.5599	22.3524	16.5636	21.9654	16.2501	16.6720	22.3877	16.5781	22.3302
ΔΔE(kcal/mol)	-	-	-	0.0037	-0.0037	0.3833	0.3099	-0.1121	-0.0390	-0.0182	0.0185

First and foremost, this is the very first time it is shown in this work a benchmark comparison of the FDB$_\beta$ method *versus* the explicit *Fields* and *point-charge* calculations. Secondly, all the point charges have an absolute value of 1.0 a.u., and as has been explained above, their position has been chosen to reproduce an electric field in the centre of the molecule of the same magnitude as the explicit homogeneous electric field studied.

$$F_Z\text{=-50 (FDB}_\beta) \equiv F_Z\text{=-50 (G16)} \equiv Q^{+1}_{bottom},\ Q^{-1}_{top} \text{ and } (Q^{+1} \rightarrow Q^{-1})$$
$$F_Z\text{=50 (FDB}_\beta) \equiv F_Z\text{=50 (G16)} \equiv Q^{+1}_{top},\ Q^{-1}_{bot} \text{ and } (Q^{-1} \rightarrow Q^{+1})$$

Focusing first on the study of the neutral water, $[H_2O]^0$, it can be seen there is a great resemblance. In other words, there is a close-to-zero ΔΔE between the **2Q** (*vide supra*) with respect to the "F$_Z$=±50 (G16)" due to the fact the electric field generated with two point charges of opposite signs is closer to a homogeneous EF than the field generated by a single point charge: the difference with respect to the homogeneous electric field decreases 30 times when two changes are used instead of one. Based on Coulomb's Law, the agreement will be even better if one uses larger point charges placed at further distances.

Next, focusing now on the $[H_2O]^+$ results, the discrepancies are similar with the exception of the

two outliers of Q^-, which have a smaller difference with the homogeneous EF than for $[H_2O]^0$ due to a compensation of effects induced by the redistribution of the positive charge in the molecule caused by the single-point negative charge.

Interestingly, for the neutral molecule, there is an excellent agreement between the values obtained with explicit EFs and the ones obtained with FDB$_\beta$. On the contrary, for the charged water, there exists a small difference caused by the origin dependence of dipole moment and first hyperpolarizability. That is why is important to compare the results of both types of calculations using the same relative Cartesian coordinates origin. We propose to place all the molecules in their centre of charge to minimise the effect of this problem. Nonetheless, it is important to remark that the FDB$_\beta$ results nicely agree with the results obtained from explicit *Field* calculations and, consequently, with the ones obtained **2Q** approach, independently of the formal charge of the system.

Ultimately, the most suitable way to experimentally impose an EF is by means of using two charged functional groups. This approach will eventually allow future designs of catalysts based on generating strong enough local EFs to enhance the catalysis.

5.2 Gas-phase CO release step

Based on what has been learnt from the previous model system, the CO release has been studied considering the different procedures capable of generating homogeneous fields: the FDB$_\beta$ method, the keyword *Field* and the **2Q** approach. Out of the three, the FDB$_\beta$ method has been used as a reference.

Table 2: CO Release within an electric field of $\pm 50(\cdot 10^{-4})$ a.u. computed with the 6-31+G(p,d) basis set.

	$\mathbf{G}_{[i.10]}$	$\mathbf{G}_{[i.2]}$	$\mathbf{G}_{[CO-MeCN]}$	$\Delta\mathbf{G}_{RLS}$ **(a.u)**	$\Delta\mathbf{G}_{RLS}$ **(kcal/mol)**	$\Delta\Delta\mathbf{G}$ **(kcal/mol)**
$\mathbf{F}_Z$**=50** (FDB$_\beta$)	-2262.5729	-2281.9901	19.4224	0.0051	3.2147	-
$\mathbf{F}_Z$**=-50** (FDB$_\beta$)	-2262.5906	-2281.9833	19.4224	0.0296	18.5680	-
$\mathbf{F}_Z$**=50** (G16)	-2262.5724	-2282.0033	19.4224	0.0054	3.4079	-0.1930
$\mathbf{F}_Z$**=-50** (G16)	-2262.5901	-2281.9900	19.4224	0.0299	18.7609	-0.1932
$\mathbf{F}_{2Q,Z}$**=50**	-2262.5717	-2281.9933	19.4224	0.0009	0.5415	2.6732
$\mathbf{F}_{2Q,Z}$**=-50**	-2262.5909	-2281.9802	19.4224	0.0331	20.7988	-2.2308

On one hand, each pair of rows of the Table are the different approaches considered to study the CO release system: the FDB$_\beta$ method, explicit fields and two charges, respectively. On the other hand, the first three columns are the corrected electronic energies of each chemical species according to the equations at the end of Section 3.1 (*vide supra*) of the Methodology.

Particularly, for [i.10], [i.2] and for [CO-MeCN] their electronic energies have been rectified in the theoretical framework of the FDB$_\beta$ method and **2Q** approach in the following manner, respectively

$$G_{i,FDB}(F) = dG_i + E_{i,FDB}(F) \tag{17}$$

$$G_{i,G16}(F) = dG_i + E_{i,G16}(F) \tag{18}$$

$$G_{i,Charge} = E_{i,Charge}(0) + dG_i - \frac{Q^+Q^-}{2(r(F)/a_o)} \tag{19}$$

where the last term of Equation (19) is the electrostatic potential generated by the point charges, analytically computed by the Gaussian16 software package. Although the last term of the expression is cancelled when an energy difference is computed, it is a healthy correction to be applied to check if there is an agreement with the FDB$_\beta$ method. The "F$_Z$=±50 (G16)" and "F$_Z$=±50 (FDB$_\beta$)" do not require extra corrections besides the conversion to Gibbs free energy and the proper computation at the centre of charge.

The second- and third-to-last columns calculate the Gibbs energy of the CO release (ΔG_{RLS}) in kcal/mol and atomic units, respectively, with the three different procedures taken into account in this Chapter. The last column simply shows the $\Delta\Delta G$ with respect to the FDB$_\beta$ method, as has been previously mentioned.

Similarly to Table 1, a full comparison of the FDB$_\beta$ method *versus* the explicit EFs and point-charge calculations, but on the reaction studied in this work. In this case, for the **2Q** calculation, the $\Delta\Delta G$ values are larger than for the water model system based on the fact the homogeneity of the field decreases with the proximity of the charges at some parts of the molecule. When stronger fields, i.e. F$_Z$=±0.01 a.u, are being considered the results given in Table 3 are obtained.

Table 3: CO Release within an electric field of ±100($\cdot 10^{-4}$) a.u. computed with the 6-31+G(p,d) basis set.

	$G_{[i.10]}$	$G_{[i.2]}$	$G_{[CO-MeCN]}$	ΔG_{RLS} (a.u)	ΔG_{RLS} (kcal/mol)	$\Delta\Delta G$ (kcal/mol)
F$_Z$=100 (FDB$_\beta$)	-2262.5737	-2282.0062	19.4312	-0.0013	-0.8230	-
F$_Z$=-100 (FDB$_\beta$)	-2262.6091	-2281.9929	19.4312	0.0474	29.7652	-
F$_Z$=100 (G16)	-2262.5720	-2282.0033	19.4316	-0.0001	-0.0639	-0.7591
F$_Z$=-100 (G16)	-2262.6188	-2281.9900	19.4316	0.0600	37.6296	-7.8644
F$_{2Q,Z}$=100	-2262.5695	-2282.0311	19.4316	-0.0134	-18.8061	17.9831
F$_{2Q,Z}$=-100	-2262.6116	-2282.0522	19.4316	0.0307	-5.6736	35.4388

Similarly to the previous Table, there is a general agreement between the FDB$_\beta$ method and the explicit *Field* calculations. However, the $\Delta\Delta G$ values obtained with point charges are astronomical with respect to either FDB$_\beta$ method. The origin of this large difference is that one of the point-charge is located at only 2.164Å to the closest atoms (3 hydrogen atoms) (see Fig. (19)).

In order to check this last statement, the single point energy of [i.2] has been recalculated using Q=±2 at a proper distance to replicate F$_Z$=±0.01 a.u (see Table 4)

Table 4: CO release within an electric field strength of ±0.01 a.u using Q=±2. Computed with the 6-31+G(p,d) basis set.

	$G_{[i.10]}$	$G_{[i.2]}$	$G_{[CO-MeCN]}$	ΔG_{RLS} (a.u)	ΔG_{RLS} (kcal/mol)	$\Delta\Delta G$ (kcal/mol)
Field=z100 (FDB$_\beta$)	-2262.5737	-2282.0062	19.4312	-0.0013	-0.8230	-
Field=z-100 (FDB$_\beta$)	-2262.6091	-2281.9929	19.4312	0.0474	29.7652	-
F$_{2Q,Z}$=100	-2262.5695	-2282.0145	19.4316	-0.0122	-7.6248	6.8018
F$_{2Q,Z}$=-100	-2262.5909	-2282.0125	19.4316	0.0319	20.0283	9.7369

As can be seen in the rightmost column the $\Delta\Delta G$ values for **2Q** values are far smaller than the

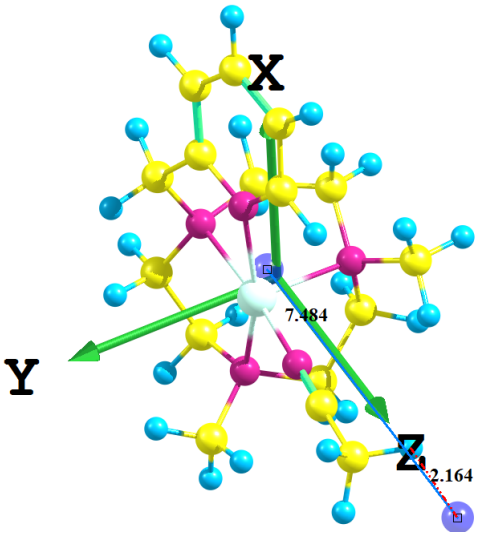

Figure 19: Proximity of [i.2]'s methyl hydrogen atoms to one of the point charges. The blue solid line is the distance to the centre of charge, while the red one is the distance to the closest hydrogen. Distances in Å.

values presented in Table 3. However, they still do not reproduce the FDB_β values. To have an even better agreement, higher charge values have to be used at longer distances to increase the homogeneous character of the electric field in the molecule.

Table 3 has also been computed, at F=±0.005 a.u, with the aug(-d^H,-$f^{C,N,O}$,-g^{Co})-cc-pVTZ basis set in order to determine which are the values obtained using the basis set used to study the mechanism (5).

Table 5: CO Release within an electric field of $\pm 50(10^{-4})$ a.u computed with aug(-d^H,-$f^{C,N,O}$,-g^{Co})-cc-pVTZ basis set and considering Q=±2 for [i.2].

	$G_{[i.10]}$	$G_{[i.2]}$	$G_{[CO-MeCN]}$	ΔG_{RLS} (a.u)	ΔG_{RLS} (kcal/mol)	$\Delta\Delta G$ (kcal/mol)
F_Z=50 (FDB_β)	-2263.0152	-2282.4346	19.4232	0.0037	2.3497	-
F_Z=-50 (FDB_β)	-2263.0325	-2282.4277	19.4232	0.0280	17.5748	-
F_Z=50 (G16)	-2263.0148	-2282.4344	19.4232	0.0036	2.2410	0.1086
F_Z=-50 (G16)	-2263.0321	-2282.4274	19.4232	0.0278	17.4659	0.1089
$F_{2Q,Z}$=50	-2263.0140	-2282.4383	19.4232	-0.0010	-0.6581	3.0077
$F_{2Q,Z}$=-50	-2263.0328	-2282.4251	19.4232	0.0310	19.4361	-1.8613

Using a more complete basis set leads to more accurate results according to the Variational Theorem. The differences between explicit electric fields and FDB_β are reduced to half in comparison with the counterpart values given in Table 2. Although using explicit point charges the differences with respect to the FDB_β method values are not smaller than in Table 2, these results confirm that the FDB_β method is a good approach to simulate the field generate by point-like charges, which can be used to design more efficient catalyst based on the usage of local EFs.

In order to compute the effect of an electric field in a mechanism computed including the effect of an implicit solvent we propose the following approximation: Sum of the field free Gibbs energy using the SMD implicit solvent model to the difference of the field-dependent and free field Gibbs free energy computed at gas phase (with the same or a smaller) basis set).

$$G_{i,SMD,BS_1}(F) \simeq G_{i,SMD,BS_1}(0) + [G_{i,BS_2}(F) - G_{i,BS_2}(0)] \tag{20}$$

This new estimation requires 3 computations, one more per species than the regular FDB$_\beta$ method, although computing the NLOPs with a smaller basis set is much cheaper than with the bigger basis set saving, then, computational time. When Equation (20) is applied to the CO release, are obtained the results presented in Table 6.

Table 6: Field-dependent approximation for the CO release in acetonitrile (SMD) using FDB$_\beta$ where BS$_1$=aug(-d^H,-f^{C,N,O},-g^{Co})-cc-pVTZ. Energies in kcal/mol.

	BS$_1$	**BS$_2$=6-31+G(d)**		**BS$_2$=6-31+(p,d)**	
	ΔG_{RLS}	ΔG_{RLS}	$\Delta\Delta G$	ΔG_{RLS}	$\Delta\Delta G$
F$_Z$=50	16.7122	17.4281	-0.7159	17.3796	-0.6674
F$_Z$=-50	36.1993	32.7207	3.4786	32.7329	3.4664
F$_Z$=100	11.7285	13.4085	-1.6799	13.3765	-1.6480
F$_Z$=-100	50.3975	43.8770	6.5205	43.9647	6.4328
F$_Z$=0	20.5660	20.5660	0.0000	20.5660	0.0000

The first column of the Table 6 contains the values obtained with FDB$_\beta$ using BS$_1$, while the third and fifth columns contain the values obtained with by FDB$_\beta$ combined with Equation (20). As can be seen, Equation (20) is a good approximation to evaluate the effect of the EF at a lower computational cost. Even though the differences are notable, the tendencies are properly reproduced and it can be used for very large chemical systems.

Ultimately, the most coherent continuation of this section would be to repeat the contents in Table 5 but applying the SMD model using acetonitrile. The main problem with this follow-up is the dielectric constant of acetonitrile being 38.8 times void's dielectric constant[44], and the size and shapes of the cavities used by SMD models. Furthermore, I would like also to study the effect on the catalysis of charged functional groups such as ammonium, imminium, carboxylate, sulfonate, etc. where the charge is not point-like but delocalised. Other options involve using more modern basis sets such as the Def2 family or DFT functionals specialised in computing NLOP, such as the Tα-LC-BLYP[45] developed by Besalú *et al.*.

Finally, I want to remark that optimising the molecules in the presence of either charges or explicit fields can also be a big step forward to see how the geometry and energy of the molecules are affected when the catalyst is attached to an electrode.

6 Conclusions

A field-free catalytic cycle based on a disproportionation mechanism has been studied at the B3LYP-D_3(SMD)/aug(-d^H,-$f^{C,N,O}$,-g^{Co})-cc-pVTZ// B3LYP-D_3(SMD)/6-31+G(d) level of theory. The effect of external electric fields on the characteristic CO release and TDTS-TDI transition has been assessed, as well, as the effects of point-charges and explicit electric fields of different strengths. From the analysis of the data obtained throughout the work, it can be concluded that:

- The FDB_β is an excellent method to estimate the effect of an electric field on the reactivity with a low computational cost associated. FDB_β is a fast method that does not require much input data.
- The studied step of the CO release can be diminished with a Z-oriented positive field (*vide supra*) whereas the TDTS-TDI can only be decreased by either a positive Y or negative Z-oriented field. On the other hand, the X-axis does not have any significant role in the studied catalysis.
- The generated 2-D diagrams are a useful tool to predict which electric field plane is relevant for catalysis. 2-D diagrams for this reaction show that the greater impact of the electric fields on the reaction occurs for fields on the YZ plane. Specifically, a field in a direction which is a linear combination of Y and Z is determined to be the most suitable to reduce the TDTS-TDI by lowering the TDTS.
- The effect of an external electric field on the Y-axis has opposite effects on the CO release and on the TDTS-TDI transition. While applying an external electric field on the Y-axis hampers the CO release, the same field actually increases the rate constant of the whole reaction mechanism due to the stabilisation of the TDTS.
- We have developed and implemented a FORTRAN95 code based on the FDB_β method that determines which is the weakest electric field necessary to reduce the TDTS-TDI barrier or the CO potential well to an arbitrary value.
- We have determined that the FDB_β method is a good approach to simulate the effect of explicit external electric fields or point charges. It is important to denote that two charges generate a more homogeneous field than only one point charge.
- We suggest an approximation that combines field-free calculations with a *big* basis set and field-dependent calculations with a *small* basis set to calculate the effect of an external electric field using the FDB_β method at a very low computational cost that can be very helpful for large chemical systems.

One of the future objectives of this work is to study the effect of charged functional groups acting on catalysis. We want to also simulate the effect of the electric fields generated by an electrode on catalysis. Further work will be needed to design a more efficient catalyst based on the acquired knowledge.

Bibliography

[1] Nikolaos Antonakakis, Ioannis Chatziantoniou, and George Filis. "Energy consumption, CO2 emissions, and economic growth: An ethical dilemma". In: *Renewable and Sustainable Energy Reviews* 68 (2017), pp. 808–824. ISSN: 1364-0321. DOI: https://doi.org/10.1016/j.rser.2016.09.105. URL: https://www.sciencedirect.com/science/article/pii/S1364032116306013.

[2] Amanda J. Morris, Gerald J. Meyer, and Etsuko Fujita. "Molecular Approaches to the Photocatalytic Reduction of Carbon Dioxide for Solar Fuels". In: *Accounts of Chemical Research* 42.12 (2009), pp. 1983–1994. DOI: 10.1021/ar9001679.

[3] American Chemical Society. *Which Gases Are Greenhouse Gases?* URL: https://www.acs.org/climatescience/greenhousegases/whichgases.html.

[4] Chad A. Meserole et al. "CO2 Absorption of IR Radiated by the Earth". In: *Journal of Chemical Education* 74.3 (1997), p. 316. DOI: 10.1021/ed074p316. URL: https://doi.org/10.1021/ed074p316.

[5] Peng-Sheng Wei et al. "Absorption coefficient of carbon dioxide across atmospheric troposphere layer". In: *Heliyon* 4.10 (2018), e00785. ISSN: 2405-8440. DOI: https://doi.org/10.1016/j.heliyon.2018.e00785. URL: https://www.sciencedirect.com/science/article/pii/S2405844018324605.

[6] P. Geerlings, F. De Proft, and W. Langenaeker. "Conceptual Density Functional Theory". In: *Chemical Reviews* 103.5 (2003). PMID: 12744694, pp. 1793–1874. DOI: 10.1021/cr990029p.

[7] Dietmar Seyferth. "The Grignard Reagents". In: *Organometallics* 28.6 (2009), pp. 1598–1605. DOI: 10.1021/om900088z. URL: https://doi.org/10.1021/om900088z.

[8] Xiaowei Song et al. "Hydrogen photogeneration catalyzed by a cobalt complex of a pentadentate aminopyridine-based ligand". In: *New J. Chem.* 39 (3 2015), pp. 1734–1741. DOI: 10.1039/C4NJ01858C. URL: http://dx.doi.org/10.1039/C4NJ01858C.

[9] Arnau Call and Julio Lloret-Fillol. "Enhancement and control of the selectivity in light-driven ketone versus water reduction using aminopyridine cobalt complexes". In: *Chem. Commun.* 54 (69 2018), pp. 9643–9646. DOI: 10.1039/C8CC04239J. URL: http://dx.doi.org/10.1039/C8CC04239J.

[10] Arnau Call et al. "Understanding light-driven H2 evolution through the electronic tuning of aminopyridine cobalt complexes". In: *Chem. Sci.* 9 (9 2018), pp. 2609–2619. DOI: 10.1039/C7SC04328G. URL: http://dx.doi.org/10.1039/C7SC04328G.

[11] Mikael Höök et al. "Hydrocarbon liquefaction: viability as a peak oil mitigation strategy". In: *Philosophical Transactions of the Royal Society A: Mathematical, Physical and Engineering Sciences* 372.2006 (2014), p. 20120319. DOI: 10.1098/rsta.2012.0319. eprint: https://royalsocietypublishing.org/doi/pdf/10.1098/rsta.2012.0319. URL: https://royalsocietypublishing.org/doi/abs/10.1098/rsta.2012.0319.

[12] Arno de Klerk. "Fischer–Tropsch Process". In: *Kirk-Othmer Encyclopedia of Chemical Technology*. John Wiley & Sons, Ltd, 2013, pp. 1–20. ISBN: 9780471238966. DOI: https://doi.org/10.1002/0471238961.fiscdekl.a01. eprint: https://onlinelibrary.wiley.com/doi/pdf/10.1002/0471238961.fiscdekl.a01. URL: https://onlinelibrary.wiley.com/doi/abs/10.1002/0471238961.fiscdekl.a01.

[13] Chiming Wang et al. "Towards developing efficient aminopyridine-based electrochemical catalysts for CO2 reduction. A density functional theory study". In: *Journal of Catalysis* 373 (2019), pp. 75–80. ISSN: 0021-9517. DOI: https://doi.org/10.1016/j.jcat.2019.03.018. URL: https://www.sciencedirect.com/science/article/pii/S0021951719301265.

[14] Shenzhen Xu and Emily A. Carter. "Theoretical Insights into Heterogeneous (Photo)electrochemical CO2 Reduction". In: *Chemical Reviews* 119.11 (2019). PMID: 30561988, pp. 6631–6669. DOI: 10.1021/acs.chemrev.8b00481.

[15] Alon Chapovetsky et al. "Electronically Modified Cobalt Aminopyridine Complexes Reveal an Orthogonal Axis for Catalytic Optimization for CO2 Reduction". In: *Inorganic Chemistry* 59.18 (2020). PMID: 32866380, pp. 13709–13718. DOI: 10.1021/acs.inorgchem.0c02086.

[16] Alon Chapovetsky et al. "Proton-Assisted Reduction of CO2 by Cobalt Aminopyridine Macrocycles". In: *Journal of the American Chemical Society* 138.18 (2016). PMID: 27092968, pp. 5765–5768. DOI: 10.1021/jacs.6b01980.

[17] Sergio Fernández et al. "A Unified Electro- and Photocatalytic CO2 to CO Reduction Mechanism with Aminopyridine Cobalt Complexes". In: *Journal of the American Chemical Society* 142.1 (2020). PMID: 31820956, pp. 120–133. DOI: 10.1021/jacs.9b06633.

[18] Mark Wrighton. "Photochemistry of metal carbonyls". In: *Chemical Reviews* 74.4 (1974), pp. 401–430. DOI: 10.1021/cr60290a001.

[19] Xiye Wang et al. "Alkane Solvent-Derived Acylation Reaction Driven by Electric Fields". In: *Journal of the American Chemical Society* 145.22 (2023). PMID: 37227235, pp. 11903–11906. DOI: 10.1021/jacs.3c02064.

[20] Fabijan Pavošević, Robert L Smith, and Angel Rubio. "Computational study on the catalytic control of endo/exo Diels-Alder reactions by cavity quantum vacuum fluctuations". en. In: *Nat. Commun.* 14.1 (May 2023), p. 2766.

[21] Nicholas S. Hill and Michelle L. Coote. "Internal Oriented Electric Fields as a Strategy for Selectively Modifying Photochemical Reactivity". In: *Journal of the American Chemical Society* 140.50 (2018), pp. 17800–17804. DOI: 10.1021/jacs.8b12009.

[22] Adam Jaroš et al. "Fullerene-Based Switching Molecular Diodes Controlled by Oriented External Electric Fields". In: *Journal of the American Chemical Society* 141.50 (2019). PMID: 31744293, pp. 19644–19654. DOI: 10.1021/jacs.9b07215.

[23] Omer Kirshenboim, Alexander Frenklah, and Sebastian Kozuch. "Switch chemistry at cryogenic conditions: quantum tunnelling under electric fields". In: *Chem. Sci.* 12 (9 2021), pp. 3179–3187. DOI: 10.1039/D0SC06295B. URL: http://dx.doi.org/10.1039/D0SC06295B.

[24] Pau Besalú-Sala et al. "Effect of external electric fields in the charge transfer rates of donor–acceptor dyads: A straightforward computational evaluation". In: *The Journal of Chemical Physics* 158.24 (June 2023). 244111. ISSN: 0021-9606. DOI: 10.1063/5.0148941. eprint: https://pubs.aip.org/aip/jcp/article-pdf/doi/10.1063/5.0148941/18016297/244111_1_5.0148941.pdf. URL: https://doi.org/10.1063/5.0148941.

[25] Sason Shaik et al. "Electric-Field Mediated Chemistry: Uncovering and Exploiting the Potential of (Oriented) Electric Fields to Exert Chemical Catalysis and Reaction Control". In: *Journal of the American Chemical Society* 142.29 (2020). PMID: 32551571, pp. 12551–12562. DOI: 10.1021/jacs.0c05128.

[26] Valerie Vaissier Welborn and Teresa Head-Gordon. "Computational Design of Synthetic Enzymes". In: *Chemical Reviews* 119.11 (2019). PMID: 30277066, pp. 6613–6630. DOI: 10.1021/acs.chemrev.8b00399.

[27] Sason Shaik et al. "Electric-Field Mediated Chemistry: Uncovering and Exploiting the Potential of (Oriented) Electric Fields to Exert Chemical Catalysis and Reaction Control". In: *Journal of the American Chemical Society* 142.29 (2020). PMID: 32551571, pp. 12551–12562. DOI: 10.1021/jacs.0c05128.

[28] Thijs Stuyver et al. "External electric field effects on chemical structure and reactivity". In: *WIREs Computational Molecular Science* 10.2 (2020), e1438. DOI: https://doi.org/10.1002/wcms.1438. URL: https://wires.onlinelibrary.wiley.com/doi/abs/10.1002/wcms.1438.

[29] Pau Besalú-Sala et al. "Fast and Simple Evaluation of the Catalysis and Selectivity Induced by External Electric Fields". In: *ACS Catalysis* 11.23 (2021), pp. 14467–14479. DOI: 10.1021/acscatal.1c04247.

[30] M. J. Frisch et al. *Gaussian˜16 Revision C.01*. Gaussian Inc. Wallingford CT. 2016.

[31] Grigoriy Zhurko. *Chemcraft - graphical program for visualization of quantum chemistry computations*. Version 1.8, build 642. 2005. URL: https://chemcraftprog.com.

[32] Roland H. Hertwig and Wolfram Koch. "On the parameterization of the local correlation functional. What is Becke-3-LYP?" In: *Chemical Physics Letters* 268.5 (1997), pp. 345–351. ISSN: 0009-2614. DOI: https://doi.org/10.1016/S0009-2614(97)00207-8.

[33] Stefan Grimme et al. "A consistent and accurate ab initio parametrization of density functional dispersion correction (DFT-D) for the 94 elements H-Pu". In: *The Journal of Chemical Physics* 132.15 (Apr. 2010). 154104. ISSN: 0021-9606. DOI: 10.1063/1.3382344. eprint: https://pubs.aip.org/aip/jcp/article-pdf/doi/10.1063/1.3382344/15684000/154104_1_online.pdf. URL: https://doi.org/10.1063/1.3382344.

[34] Aleksandr V. Marenich, Christopher J. Cramer, and Donald G. Truhlar. "Universal Solvation Model Based on Solute Electron Density and on a Continuum Model of the Solvent Defined by the Bulk Dielectric Constant and Atomic Surface Tensions". In: *The Journal of Physical Chemistry B* 113.18 (2009). PMID: 19366259, pp. 6378–6396. DOI: 10.1021/jp810292n.

[35] Benjamin P. Pritchard et al. "New Basis Set Exchange: An Open, Up-to-Date Resource for the Molecular Sciences Community". In: *Journal of Chemical Information and Modeling* 59.11 (2019). PMID: 31600445, pp. 4814–4820. DOI: 10.1021/acs.jcim.9b00725.

[36] Paul N. Butcher and David Cotter. *The Elements of Nonlinear Optics*. Cambridge Studies in Modern Optics. Cambridge University Press, 1990. DOI: 10.1017/CBO9781139167994.

[37] Y.R. Shen. *The Principles of Nonlinear Optics*. Wiley classics library. Wiley, 2003. ISBN: 9780471430803. URL: https://books.google.es/books?id=xeg9AQAAIAAJ.

[38] Keith E. Laidig and Richard F. W. Bader. "Properties of atoms in molecules: Atomic polarizabilities". In: *The Journal of Chemical Physics* 93.10 (Nov. 1990), pp. 7213–7224. ISSN: 0021-9606. DOI: 10.1063/1.459444. eprint: https://pubs.aip.org/aip/jcp/article-pdf/93/10/7213/11221412/7213_1_online.pdf. URL: https://doi.org/10.1063/1.459444.

[39] Marc Montilla, Josep M. Luis, and Pedro Salvador. "Origin-Independent Decomposition of the Static Polarizability". In: *Journal of Chemical Theory and Computation* 17.2 (2021). PMID: 33439029, pp. 1098–1105. DOI: 10.1021/acs.jctc.0c00926.

[40] Graham J. B. Hurst, Michel Dupuis, and Enrico Clementi. "Ab initio analytic polarizability, first and second hyperpolarizabilities of large conjugated organic molecules: Applications to polyenes C4H6 to C22H24". In: *The Journal of Chemical Physics* 89.1 (July 1988), pp. 385–395. ISSN: 0021-9606. DOI: 10.1063/1.455480. eprint: https://pubs.aip.org/aip/jcp/article-pdf/89/1/385/11267958/385_1_online.pdf. URL: https://doi.org/10.1063/1.455480.

[41] Robert Zaleśny et al. "On the physical origins of interaction-induced vibrational (hyper)polarizabilities". In: *Phys. Chem. Chem. Phys.* 18 (32 2016), pp. 22467–22477. DOI: 10.1039/C6CP02500E. URL: http://dx.doi.org/10.1039/C6CP02500E.

[42] Josep M. Luis, Miquel Duran, and José L. Andrés. "A systematic and feasible method for computing nuclear contributions to electrical properties of polyatomic molecules". In: *The Journal of Chemical Physics* 107.5 (Aug. 1997), pp. 1501–1512. ISSN: 0021-9606. DOI: 10.1063/1.474503. URL: https://doi.org/10.1063/1.474503.

[43] Sebastian Kozuch and Sason Shaik. "How to Conceptualize Catalytic Cycles? The Energetic Span Model". In: *Accounts of Chemical Research* 44.2 (2011). PMID: 21067215, pp. 101–110. DOI: 10.1021/ar1000956.

[44] https://pubchem.ncbi.nlm.nih.gov/compound/Acetonitrile.. Accessed: 2023-6-12.

[45] Pau Besalú-Sala et al. "A new tuned range-separated density functional for the accurate calculation of second hyperpolarizabilities". In: *Phys. Chem. Chem. Phys.* 22 (21 2020), pp. 11871–11880. DOI: 10.1039/D0CP01291B. URL: http://dx.doi.org/10.1039/D0CP01291B.

Agraïments

A la meva família. Vull començar pel meu pare, Josep Pey Salvi, el qual va defallir l'any passat però sempre va procurar que jo pogués estudiar, i la meva mare Mª Assumpció Costa Gou per recolzar-me durant la carrera. Pel que ha hagut d'escoltar la meva mare durant la carrera, crec que es podria merèixer un grau honorari en Química. També agrair als meus germans Francesc Pey Costa i Josep Pey Costa per sentir-me parlar (no tant) de la carrera, o de química, i quasi mai no entendre de què parlava.

Vull agrair especialment als meus millors amics de Figueres Jordi Barrera Perxés, Alain Homs Espinosa i Daniel Vázquez Samos que han estat al meu costat durant quasi la meitat de la meva vida. En una mica d'excepció d'en Jordi, ells tampoc no m'han entès mai en qüestió de Química però son els meus millors amics, i no els canviaria mai per res del món. Per altra banda, qui sí m'ha seguit en aquest aspecte son els millors amics que he fet durant els quatre anys de la carrera: l'Aleix Masbernat Solbes-Godina i l'Elisabeth González García; si amb ells no he parlat cada dia dels curs acadèmic, poc en faltaria.

No voldria endescuidar-me'n tampoc dels altres amics amb qui m'he queixat moltes vegades que les assignatures no m'agradaven, amb qui he compartit hores d'estudi i de descans, i he repetit moltes vegades que no em veia capaç d'arribar aquí. Aquí hi vull mencionar a l'Esther Alonso Cañada, la Nora Alpuente Jiménez, en Mario Bonachea Gener i la Maria Pagès Corominas.

També remarcar, en cap ordre en concret, a les amistats més properes alienes al grau de Química amb qui també he anat explicant alegries i penúries com l'Aimar Guillén Blánquez, la Paula Ruiz Duran, la Mont Xinmao Juanola Marcé, en Joan Romà Dot Codina i en Jan Figueras Gibert.

Hi ha tres professors en concret que m'han marcat molt durant la meva carrera estudiantil. A la Xon Coll, amb qui em vaig sentir molt recolzat durant el meu període de dubte entre estudiar Física o Química i qui em va transmetre gran passió i amor per les matemàtiques. A en Carles Llensa, qui em va introduir al món de la programació amb C++ durant el Treball de Recerca de Batxillerat i em va fer endinsar una mica més que la Xon en les matemàtiques. Per últim, però no menys important, a la Dolors Corcoll, la meva professora de Física i Química a Batxillerat, i que em coneix, pràcticament, de tota la meva vida, que va ser la primera persona en saber que estudiaria Química i algú que també em va recolzar molt durant Batxillerat.

Finalment, vull donar els majors agraïments al meu tutor de Treball de Fi de Grau, Dr. Josep Maria Luis Luis, i al Dr. Julio Lloret-Fillol tant per confiar en mi el suficient com per donar-me un projecte d'aquest estatus com per acollir-me sota la seva tutela i, sobretot, al meu mentor (i futur Doctor) Pau Besalú Sala per no ser només un mentor sinó també un amic.